Journal of Structural Geology, Vol. 15, No. 9/10, pp. 1097 to 1121, 1993
Printed in Great Britain

0191-8141/93 $06.00+0.00

Strength and anisotropy of foliated rocks with varied mica contents

WILLIAM T. SHEA, JR* and ANDREAS K. KRONENBERG†

Center for Tectonophysics, Texas A&M University College Station, TX 77843, U.S.A.

(*Received* 2 *July* 1992; *accepted in revised form* 4 *March* 1993)

Abstract—We have shortened 15 schists and gneisses with varying compositions (15–75% mica by volume) at angles (β) of 45° and 90° to foliation (S) to investigate the influence of micas on the strength and anisotropy of foliated rocks. At the conditions tested (T = 25°C, P_c = 200 MPa and $\dot{\varepsilon} = 10^{-5}$ s^{-1}), compressive strengths vary by a factor >4 in the β = 45° and β = 90° orientations, and individual rock types exhibit directional responses ranging from isotropic to strongly anisotropic. Trends of decreasing strength, decreasing anisotropy and increasing ductility are observed with increasing mica content. Strains in all samples were localized within inclined shear zones, accommodated by dislocation slip and grain-scale microkinking in micas and microcracking in all other silicates. Stress–strain response and grain-scale deformation microstructures both indicate that mechanical behavior is strongly influenced by the concentration and spatial arrangement of micas. Shear zone formation is associated either with discrete brittle fracture, transitional strain softening or steady-strength ductile shear. In both brittle and transitional samples, extensive microcracking of strong quartzo-feldspathic bridges occurs, and stress drop magnitudes decrease with decreasing spacing and increasing overlap of adjacent, critically-oriented micas. Steady-strength ductile shear zones develop in samples containing domains of interconnected micas, and isotropic mechanical response is observed in those in which micas are contiguous in nearly all directions.

INTRODUCTION

MICROSTRUCTURES of micas and related layer-silicates associated with dislocation glide and kinking, diffusion-assisted recovery, and dynamic recrystallization are commonly observed in foliated rocks deformed over a wide range of crustal depths (Hobbs *et al.* 1976, Wilson & Bell 1979, Bell & Wilson 1981, Vernon *et al.* 1983, Bell *et al.* 1986, Bons 1988, Goodwin & Wenk 1990, Kanaori *et al.* 1991). Deformation experiments on single crystals have shown that, at laboratory conditions, plastic flow involving basal slip and kinking occurs at low differential stresses (generally <200 MPa) that depend only weakly upon temperature and strain rate (Etheridge *et al.* 1973, Kronenberg *et al.* 1990, Mares & Kronenberg 1993). At relatively shallow crustal depths, where dislocation mobility in other coexisting silicate minerals is limited, phyllosilicates may therefore constitute the weakest phase in a wide variety of common crustal rocks. Several recent theoretical studies (Jordan 1988, Handy 1990, Tullis *et al.* 1991) have shown that the strengths of polyphase aggregates depend strongly on the volume proportion of the weakest phase, and strength vs composition relations for many two-phase aggregates generally confirm these model predictions (Price 1982, Burg & Wilson, 1987, Jordan 1987, Logan & Rauenzahn 1987, Ross *et al.* 1987). Despite the widespread occurrence of micas in the crust, however, there have been few experimental attempts to investigate specifically the extent to which micas influence strengths and modes of deformation of crustal rocks.

Experimental data have been gathered for mica-bearing polycrystals primarily for the purpose of defining mechanical anisotropies. Strength anisotropies of foliated rocks can be pronounced, with compressive strengths varying as a function of angle β measured between the foliation (S) and compression axis. Samples loaded in orientations that result in large shear stresses resolved on the foliation plane are often several times weaker than those shortened parallel or perpendicular to S (Jaeger 1960, Donath 1961, 1964, 1972, Borg & Handin 1966, Paterson & Weiss 1966, McLamore & Gray 1967, McCabe & Koerner 1975, Gottschalk *et al.* 1990). Despite similarities in the variation of differential stress with orientation among rock types, published compressive strengths for samples shortened in a given orientation vary widely (Fig. 1a), presumably due to differences in texture and composition. Room temperature results for samples shortened at 45° and 90° to foliation span a range of several hundred MPa at any given confining pressure to 500 MPa, and pressure dependencies of strength revealed by the slopes of these differential stress-confining pressure plots differ significantly among rock types in both orientations. Anisotropy coefficients [defined here as the ratio of compressive strengths, σ_d, of samples shortened at 90° and 45° to foliation; $\sigma_d(\beta = 90)/\sigma_d(\beta = 45)$] for these same rocks also differ markedly over a range of confining pressures (Fig. 1b). These data suggest that microstructural sources of anisotropy in foliated rocks may be diverse.

Several different macroscopic descriptions of the orientational strength dependence of foliated rocks have been proposed and compared with experimental results (Fig. 2). The simplest models treat foliation as a unique, anomalous plane of weakness (Jaeger 1960, Donath 1961), while transversely anisotropic models predict continuously varying shear strengths as a function of β or

*Current address: Exxon Production Research Co., P.O. Box 2189, Houston, TX 77252, U.S.A.
†Also at Department of Geophysics.

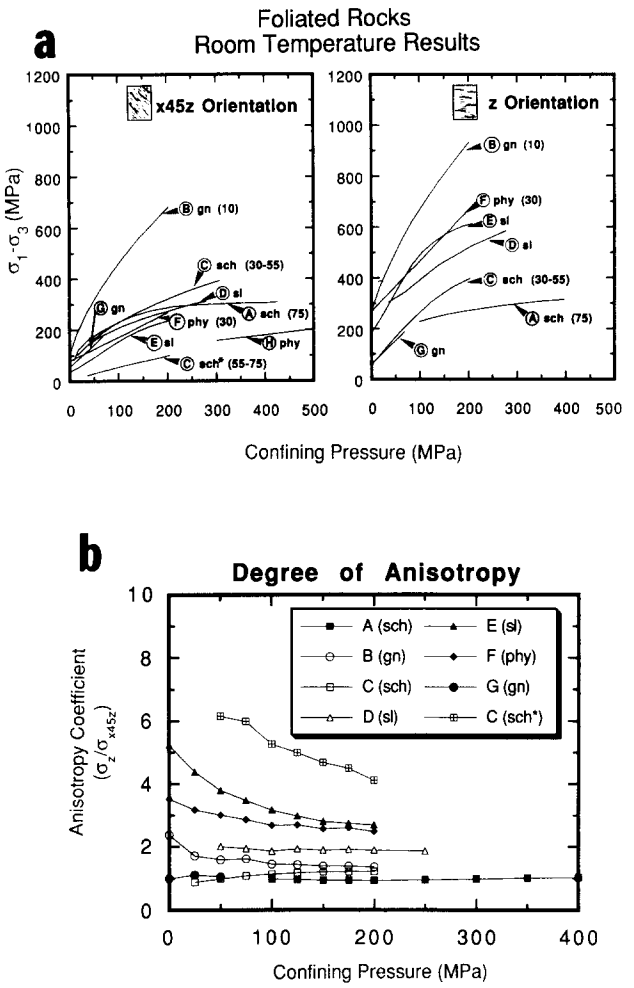

Fig. 1. Differences in the anisotropic mechanical behavior of foliated rocks, as reported in previous studies. Data for slates (sl), phyllites (phy), schists (sch) and gneisses (gn) are shown. (a) Differential stress $\sigma_1 - \sigma_3$ (fracture strength or steady flow stress) as a function of confining pressure ($P_c = \sigma_3$) for samples shortened at 45° ($x45z$ orientation) and 90° (z orientation) to the mesoscopic foliation (S). Where they have been reported, bulk mica contents (as % of sample volume) are given in parentheses. (b) Anisotropy coefficients of rock types in (a), defined as the ratio of differential stresses ($\sigma = \sigma_1 - \sigma_3$) measured in the z and $x45z$ orientations (σ_z/σ_{x45z}). Data are labeled: (A) biotite schist (Shea & Kronenberg 1992); (B) Four Mile gneiss (Gottschalk *et al.* 1990); (C) Wissahickon schist (McCabe & Koerner 1975) (data marked with an * refer only to samples with large, throughgoing mica veins); (D) slate, (McLamore & Gray 1967); (E) Martinsburg slate (Donath 1966); (F) Moretown phyllite (Donath 1972); (G) schistose gneiss (Deklotz *et al.* 1966); (H) Nelligen phyllite (Paterson & Weiss 1966).

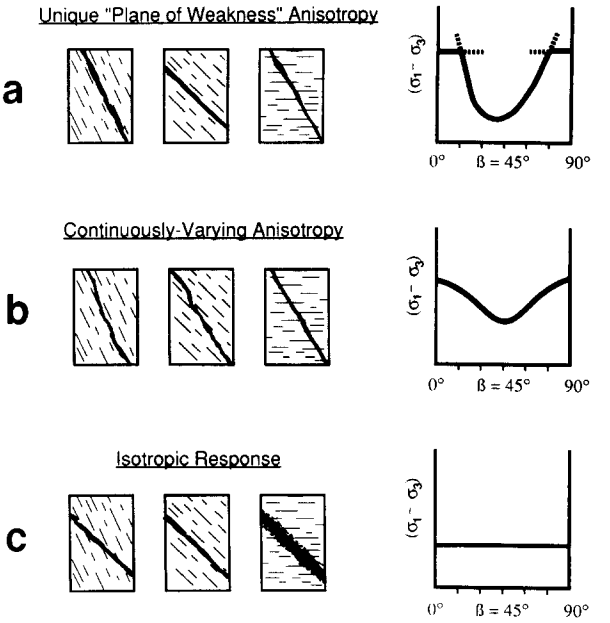

Fig. 2. Descriptions of deformation mode and mechanical anisotropy of foliated rocks. (a) Ultimate strength $\sigma_1 - \sigma_3$ as a function of β (the angle between the foliation plane and the compression direction in conventional triaxial tests) for model that assumes that foliation is a unique 'plane of weakness' in an otherwise isotropic rock. Failure is expected to occur by sliding along the foliation at intermediate values of β, and by throughgoing fracture development in more extreme orientations. (b) Strength $\sigma_1 - \sigma_3$ varies continuously with β for more general, three-dimensional models of anisotropy. Failure and foliation planes do not necessarily coincide, even at intermediate values of β. (c) Although foliated rocks have commonly been assumed to be anisotropic, results for some mica-rich schists (Shea & Kronenberg 1992) appear to require a nearly isotropic yield criterion.

more general orientations (Jaeger 1960, McLamore & Gray 1967, Pariseau 1972, Ashour 1988, Karr *et al.* 1989). More complex, three-dimensional failure envelopes have also been proposed; these predict shear zone orientations that are not necessarily parallel to the foliation plane (Pariseau 1972, Ashour 1988, Karr *et al.* 1989, Gottschalk *et al.* 1990). Although anisotropic behavior is commonly assumed for foliated mica-rich rocks, some foliated rocks appear to be described by nearly isotropic relations (Shea & Kronenberg 1992).

Ultimately, the mechanisms that give rise to different orientational dependencies of strength must be identified from further experimental work and microstructural studies of foliated rocks. Yield criteria that have been proposed to describe the behavior of anisotropic rocks can then be evaluated in terms of their consistency with these mechanisms. Certain functional forms of the stress vs orientation curve may be associated with distinct variations in deformation mode with shortening direction that may only arise in rocks with limited ranges of textures and compositions. Changes in strength, stress–strain response and mode of deformation need to be evaluated as a function of shortening direction in different rock types, and related to textural and compositional characteristics of the starting materials.

In this paper we explore the effects of compositional and textural factors on the anisotropic mechanical behavior of foliated, mica-bearing rocks. We deformed 15 different starting materials with a wide variety of initial fabrics, and mica contents ranging from 15 to 75% by volume, in an effort to correlate starting material characteristics (e.g. mica content, strength of preferred orientation and phase dispersion) with mechanical response and deformation mechanisms. We did not attempt to determine the complete orientational dependence of strength for any rock type. Instead, samples were shortened at angles of either 45° or 90° to mesoscopic foliations, to capture near-minimum and maximum compressive strengths. Anisotropy coefficients determined from 45° and 90° results for the same rock type provide a relative measure of the orientational dependencies of strength of the different starting materials, and enabled us to identify variables that lead to anisotropic or isotropic response. All experiments

were performed at room temperature, 200 MPa confining pressure, and a constant strain rate of 1×10^{-5} s^{-1}; however, the results should be applicable over a range of conditions since neither the relative strengths nor degrees of anisotropy of previously studied rock types vary significantly as a function of confining pressure (Fig. 1).

STARTING MATERIAL

Sample sources

We selected 15 different schists and gneisses from field outcrops and from unweathered cores recovered from two shallow NSF drill holes through mica-bearing crystalline basement rocks in the southern Appalachians, U.S.A. (kindly provided by N.I. Christensen). These cores penetrated sections of phyllonites from the Brevard fault zone (NSF Drill Hole 2) and gneisses from the eastern Blue Ridge province (NSF Drill Hole 4); location maps and detailed petrologic descriptions of the two cores are given by Williams *et al.* (1987). Christensen & Szymanski (1988) measured compressional wave velocities in many of the same core intervals we selected in NSF Drill Hole 2, and documented significant velocity anisotropies related to strong phyllosilicate preferred orientations. Sources, locations, and detailed descriptions of the fabric characteristics of all starting materials are given in Table 1.

Fabric and compositional characteristics

In the selection of starting materials, we sought to maximize variations in the concentration, size, preferred orientation, and spatial arrangement of mica grains so that we might sample the range of mechanical behavior exhibited by foliated, mica-bearing rocks. In addition, we attempted to minimize variations in the mineralogy of other stronger phases by restricting our choices to quartzo-feldspathic rocks containing variable amounts of biotite and/or muscovite; other (non-mica) phases rarely comprise more than 10 vol % of any starting material. Some chlorite was also present in selected samples.

At the experimental conditions of this study, muscovite is weaker than biotite (Mares & Kronenberg 1993). Chlorite may be weaker than biotite, as well (Shea & Kronenberg 1992). However, microstructural observations of our deformed schist samples suggest that the dominant deformation mechanisms in all three phyllosilicates are the same, with each behaving as a weak inclusion embedded within a stronger host. In these room temperature tests, quartz and feldspar both deformed solely by microcracking. Although microstructural studies of granitic rocks deformed experimentally and naturally have suggested that feldspar is more susceptible to fracture than quartz (Tullis & Yund 1977, Evans 1988, 1990, Janecke & Evans 1988), we did not attempt to identify the extent to which variations in the quartz to feldspar ratio influences the bulk response of the mica-rich rocks tested in this study. The approximate composition of each sample tested (based on point counts of at least 400 grains per specimen) is listed in Table 2.

Mesoscopic foliations (S) in all starting materials are defined by a compositional segregation into alternating domains of high and low mica content (Fig. 3). All samples possess some degree of mica preferred orientation, and the average trend of mica (001) planes is generally parallel to the compositionally defined foliation. In some samples, however, micas may be only weakly aligned, or inclined (by up to 40°) to the overall trend of mica-rich zones (Fig. 5). The mean grain sizes of quartz and the feldspars tend to scale with the dimensions of micas; however, microstructural observations of the deformed samples indicate that these variations among the starting materials are not as important as differences in the dimensions and distributions of micas and mica clusters.

In rocks with low mica contents (<20 vol %) individual mica grains may be dispersed and entirely isolated in an interconnected framework of other phases, but in most starting materials segregation occurs at some scale. The geometries of mica segregations and the scales at which segregation occurs both vary considerably among starting materials, and the degree of mica segregation generally increases with increasing bulk mica content. Micas may be concentrated into isolated lenticular clusters (Figs. 3a–c), irregular films (Fig. 3d) and discrete seams (Figs. 3e–f); thicknesses of individual segregations and spacings between them range from $<100\,\mu$m to several millimeters. The average and maximum lengths of mica segregations also vary significantly among starting materials (Table 1); in many highly segregated rocks continuous layers or seams run across the diameter of (8 mm wide) samples.

Although most of the starting materials have experienced complex deformation histories, mica grains typically have highly recovered optical microstructures, and lack sharp deformation and kink bands. All constituent phases of the starting materials contain populations of pre-existing microcracks. Quartz and feldspar often show grain shape preferred orientations parallel to S, and exhibit varying degrees of undulatory extinction, subgrain development, and grain refinement. However, these inherited microstructures can be readily distinguished from those that developed during the deformation experiments.

Previous studies have shown that variations in strength and deformation mode of schists and gneisses can be related to the proportional number of mica grains oriented favorably for kinking and glide in samples shortened at varying orientations to the foliation plane (Borg & Handin 1966, Gottschalk *et al.* 1990, Shea & Kronenberg 1992). We used a universal stage to measure poles to mica {001} cleavage orientations in selected samples, in order to compare the patterns and strengths of preferred orientation among rock types, and investigate relationships between preferred orientations and mechanical anisotropy in a wider range of

rocks than had been studied previously. Stereographic projections of these measurements are shown in Fig. 5.

EXPERIMENTAL METHODS

Apparatus

Constant strain-rate compression experiments were performed on ~20.3 mm long and 8.8 mm diameter right cylindrical samples, using a Heard-type argon gas apparatus. All experiments were conducted at room temperature (~25°C), a confining pressure of 200 MPa, and a strain rate of $\sim 1 \times 10^{-5}$ s^{-1} on oven dry (~110°C) samples, to strains ranging up to 12% axial shortening. Samples were not vented to the atmosphere. Raw mechanical data were corrected for apparatus distortion, as well as the strength of the 0.025 mm thick copper jackets that isolated samples from the confining medium. Corrections to differential stress were made for changing cross-sectional areas of samples during shortening, by

Table 1. Sources and descriptions of rocks tested

Rock type	Depth (m)	Mica preferred orientation	Mica grain size*	Foliation description†
Appalachian drill cores				
NSF Drill Hole 2 (Brevard fault zone core)				
Schist	29.0	Strong	Very fine	Domainal fabric.‡ Matrix of intermixed QF§/aligned micas, with discontinuous‖ lenticular mica films (<1 mm wide) interspersed.
Schist	43.6	Strong	Very fine	Nearly homogeneous fabric. Aligned micas isolated in QF framework, with weak segregation into mm-spaced mica-rich and mica-poor zones parallel to *S*.
Schist	84.4	Strong	Fine	Segregated layering. Aligned micas isolated in QF framework, with continuous‖ mica layers (1–2 mm wide) interspersed.
Schist	126.8	Strong	Very fine–fine	Domainal fabric. Aligned micas isolated in QF framework, with discontinuous lenticular mica films (<0.5 mm wide) interspersed.
NSF Drill Hole 4 (Eastern Blue Ridge core)				
Gneiss	75.6	Strong	Medium–coarse	Domainal fabric. Aligned micas isolated in QF framework, with discontinuous-to-continuous mica lenses (0.5–2 mm wide) interspersed.
Gneiss	170.4	Strong	Medium	Nearly-homogeneous fabric.‡ Aligned micas isolated in QF framework, with weak segregation into mm-spaced mica-rich and mica-poor zones parallel to *S*.
Gneiss	234.1	Moderate	Fine–medium	Gneissic layering. Irregular, discontinuous mica and QF clusters (<1 mm wide) elongate parallel to *S*.
Gneiss	241.8	Strong	Medium	Gneissic layering.‡ Discontinuous mica lenses (<1 mm wide) dispersed in QF matrix.

Rock type	Formation	Locality	Mica preferred orientation	Mica grain size*	Foliation description†
Outcrop samples					
Schist	Honey I	Llano Co, TX	Strong¶	Very fine–fine	Domainal fabric.‡ Homogeneous distribution of discontinuous lenticular mica and QF domains (<100 μm wide). Maximum concentration of mica {001} planes inclined at ~15° to *S*, defined by mm-scale color banding (resulting from slight variations in biotite concentration).
Schist	Honey II	Llano Co, TX	Strong¶	Very fine	Domainal fabric. Zones of intermixed QF/aligned micas, separated by irregular, discontinuous-to-continuous mica films (<0.5 mm wide).
Schist	Sandy	Llano Co, TX	Strong¶	Fine	Differentiated layering.‡ Continuous, planar mica-rich and QF-rich interlayers (0.2–1 mm wide).
Gneiss	Rough Ridge	Llano Co, TX	Moderate¶	Very fine–fine	Gneissic layering. Irregular, discontinuous-to-continuous mica-rich and QF-rich layers (0.5–1 mm wide). Maximum concentration of mica {001} planes inclined at ~40° to layering.
Schist	Riggins	Idaho Co, ID (45°26′N/ 116°18″W)	Weak/ strong¶	Fine	Segregated layering.‡ Continuous seams (<3 mm wide) of strongly-aligned micas separating matrix of micas (with weak alignment of mica {001}planes) and isolated epidote grains.
Schist	Hartland	Torrington, CT	Weak¶	Fine–medium	Granoblastic texture. Foliation defined only by weak alignment of mica {001} planes.

*Relative grain size classification is based on average length (long dimension) of individual mica platelets. Very fine, <0.2 mm; fine, 0.2–0.5 mm; medium, 0.5–1 mm; coarse; >1 mm.

†Except where otherwise indicated, foliation (*S*) is defined by statistical alignment of mica {001} planes and/or the trend of distinct mica films, lenses or planar layers. In some samples, a grain-flattening fabric is developed within other silicate phases (e.g. quartz and/or feldspar).

‡Micrograph of undeformed starting material is shown in Fig. 3.

§QF = quartzo-feldspathic.

‖'Discontinuous' and 'continuous' are length scale-defined relative to sample dimensions, and refer to mineral segregations that are longer or shorter than the 8 mm sample diameter, respectively.

¶Crystallographic preferred orientation of micas shown in Fig. 5.

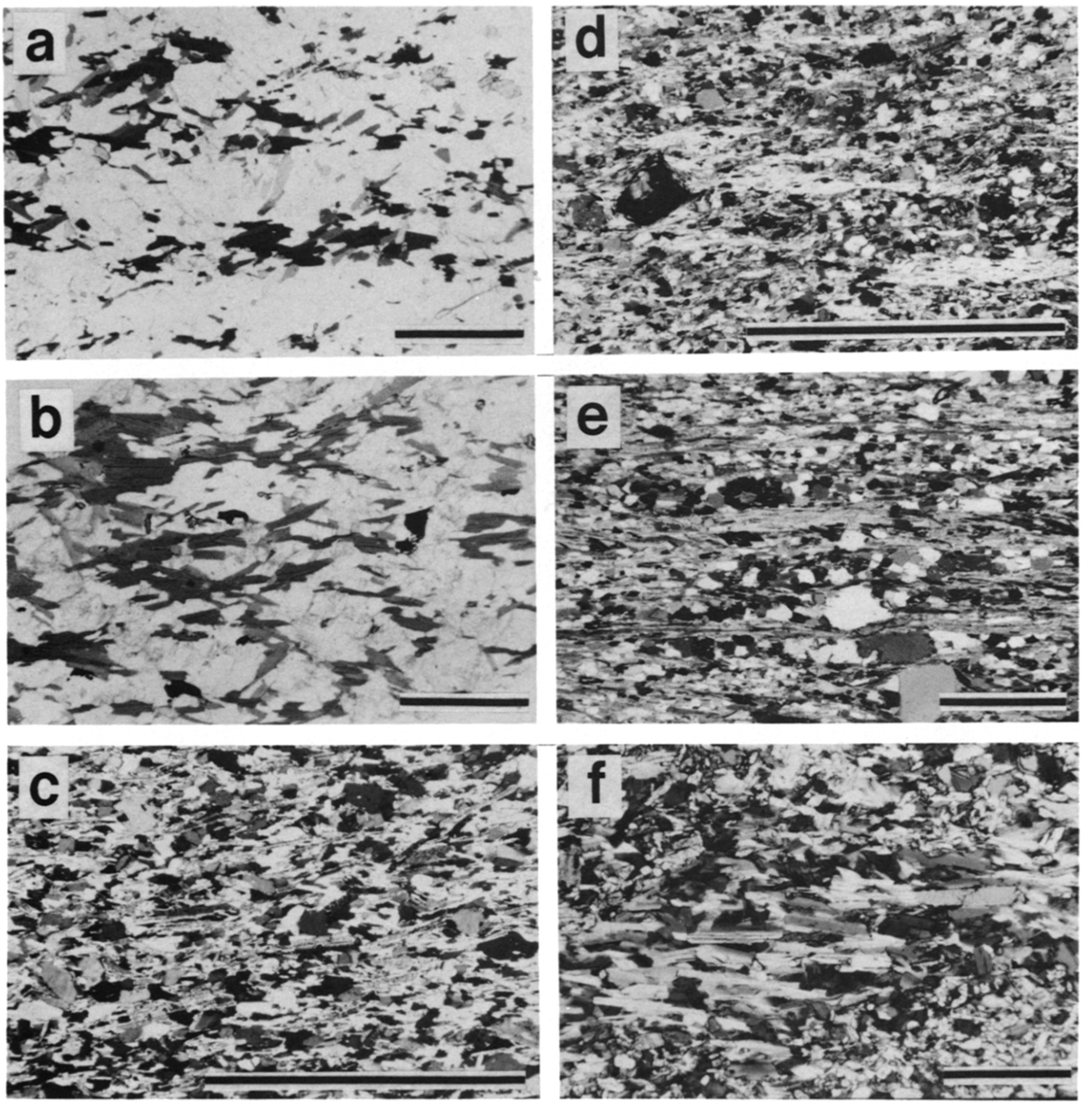

Fig. 3. Optical micrographs of selected starting materials used in this study. Micrographs illustrate distinct differences in the geometries and spacings of multigranular mica segregations, and can be cross-referenced with the textural descriptions in Table 1. In all micrographs, foliation (S) is horizontal and scale bars = 1 mm; ppl refers to plane polarized light and xn refers to crossed nicols. (a) NSF Drill Hole 4—170.4 m (ppl); (b) NSF Drill Hole 4—74.6 m (ppl); (c) Honey Formation I (xn); (d) NSF Drill Hole 2—29.0 m (xn); (e) Sandy Formation (xn); (f) Riggins Formation (ppl).

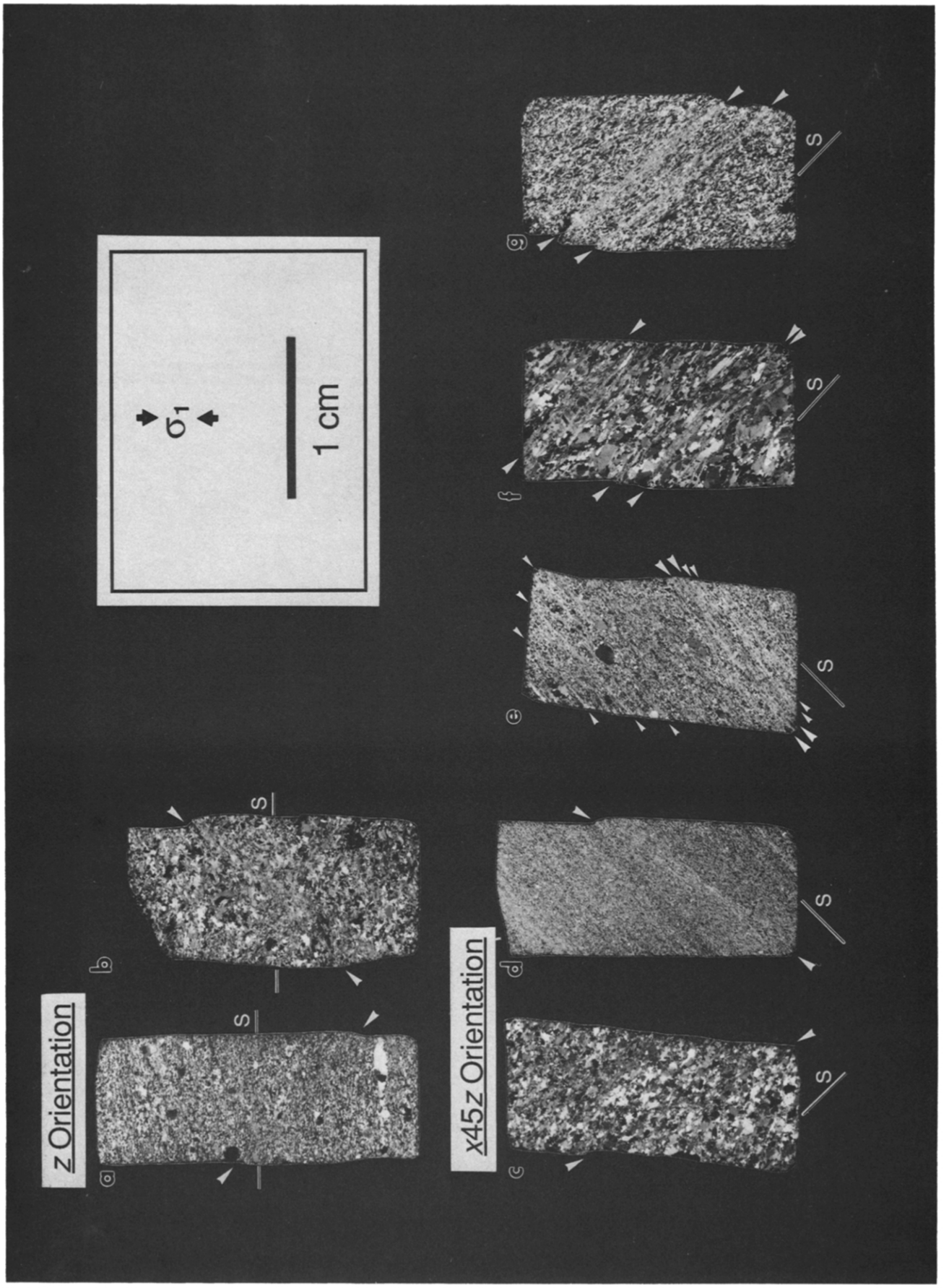

Fig. 4. Whole-sample micrographs (viewed through crossed polarizing filters) showing deformation localized within shear zones in samples shortened (a&b) perpendicular to S (orientation z) and (c–g) at 45° to S (orientation x45z). The trace of S is shown on all micrographs, and white arrows locate the traces of shear zones (smaller arrows indicate zones of limited displacement). (a) Sandy Formation, experimental sample DMS-Z1, exhibited brittle mechanical response, as described in the text; (b) Hartland Formation, sample H770-Z1, deformed by ductile shear. (c) NSF Drill Hole 4—170.4 m, sample A4-559-1, exhibited brittle behavior in the x45z orientation; (d) Honey Formation I, sample MS-S1, showed transitional behavior; (e)–(g) deformed by ductile shear: (e) Sandy Formation, sample DMS-S1; (f) NSF Drill Hole 4—74.6 m (sample A4-248-2); (g) Riggins Formation schist (sample BS-S7, Shea & Kronenberg 1992).

assuming that deformed samples remain cylinders of constant volume. In most experiments, deformation occurred by brittle faulting or ductile shear within one or more narrow zones, and uncertainties in differential stress of ± 5% may therefore result in this correction at the largest strains.

Sample preparation

Samples were cored from starting materials at 45° and 90° to their mesoscopic foliation (and to their lineation, when it could be identified in hand samples), with the resulting sample orientations denoted *x*45*z* and *z*, respectively. We were not able to obtain samples of suitable length with axes normal to foliation (orientation *z*) from many of the Appalachian Drill Hole cores.

Standard coring techniques tended to break cores parallel to foliation for many of the starting materials with prominent planar layers of strongly aligned micas (e.g. the Sandy and Honey Formation (Unit II) schists). For these materials, rectangular blocks of schist were impregnated with napthalene prior to coring (adapting techniques of G. Bussod personal communication) to fill open cleavage and fractures and prevent separation along foliation. Blocks were immersed in molten napthalene (T~150°C) and cooled. Once the napthalene crystallized, samples were cored and their ends ground perpendicular to their axes. Samples were then heated in air at ~120°C for at least 24 h to remove any napthalene residing in pore spaces.

Microstructural observations

Following deformation, all samples were impregnated with epoxy resin and standard (~30 μm thick) optical thin sections (oriented parallel to the compression axis and normal to identifiable faults or shear zones) were prepared for microstructural examination. To resolve fine-scale deformation microstructures within the micas in more detail, ultra-thin (<5 μm thick) sections were prepared from selected samples.

Thin foils for transmission electron microscopy (TEM) were prepared by ion milling and were examined using a Phillips 400T instrument at an accelerating voltage of 120 kV. A cryogenic TEM specimen holder was used to minimize radiation damage of the samples.

MECHANICAL RESULTS

The results of experiments performed on samples with compression axes directed at 90° (orientation *z*) and 45° (orientation *x*45*z*) to foliation are assembled in Table 3. In all experiments, strains were localized within narrow (sub-mm to a few mm wide) throughgoing shear zones that transect samples at angles of 28–50° (Fig. 4). Shear zones cross-cut foliation at high angles in *z* orientation samples (Figs. 4a & b), but are oriented at shallow angles to *S* (Figs. 4c & d) or localized along foliation planes (Figs. 4e–g) in *x*45*z* samples. Multiple shear zones with different amounts of displacement commonly

Table 2. Bulk composition (by volume %) of experimental samples*

Experiment number	Formation/ source	Mu†	Bt‡	QF§	Other major‖ phases	Total phyllosilicate content
*x*45*z* orientation						
A2-095-01	DH 2—29 m	24	20	54	—	44
A2-143-01	DH 2—43.6 m	15	1	83	—	16
A2-277-01	DH 2—84.4 m	34	—	54	chlorite (10), garnet (3)	44
A2-416-01.S	DH 2—126.8 m	11	13	69	calcite (3), chlorite (3)	27
A4-248-01	DH 4—74.6 m	7	18	74	—	25
A4-248-02	DH 4—74.6 m	21	27	52	—	48
A4-559-01	DH 4—170.4 m	—	21	76	epidote (3)	21
A4-768-01.S	DH 4—234.1 m	1	27	68	sphene (3)	28
A4-793-01	DH 4—241.8 m	3	30	66	—	33
BG-S01	Rough Ridge	—	37	63	—	37
BS-S01	Riggins	—	76	3	epidote (19)	76
CLS-S1	Honey II	16	14	69	—	30
DMS-S01	Sandy	25	21	53	—	46
MS-S01	Honey I	36	10	51	—	46
z orientation						
A2-416-03.Z	DH 2—126.8 m	16	11	63	calcite (6), chlorite (3)	30
A4-768-02.Z	DH 4—234.1 m	—	35	61	—	35
BG-Z01	Rough Ridge	—	42	58	—	42
BG-Z02	Rough Ridge	—	38	62	—	38
BS-Z07	Riggins	—	78	3	epidote (17)	78
CLS-Z02	Honey II	15	16	69	—	31
DMS-Z01	Sandy	17	17	66	—	34
H770-Z01	Hartland	13	50	27	amphibole (9)	63
MS-Z01	Honey I	35	10	49	opaques (3)	45

*As determined from point counts on ~400 grains per sample.
†Mu = muscovite.
‡Bt = biotite.
§QF = quartz–feldspar (undifferentiated).
‖ In excess of 2 vol %.

formed in those $x45z$ samples in which strains localized parallel to S.

Stress–strain behavior

Although sample-scale modes of deformation were similar in the two orientations tested, the corresponding stress–strain response varied widely with rock type, as well as with orientation for a given rock type. Differential stress–axial strain curves for all samples shortened in the z and $x45z$ orientations are shown in Fig. 6. In both orientations, samples show one of three distinct classes of mechanical response. The stress–strain response of rocks with low mica contents is characteristic of brittle behavior (Figs. 6a & d), showing a linear elastic rise in differential stress, followed by inelastic deformation leading to a peak stress and a sudden stress drop associated with the formation of a single macroscopic fracture. Samples of higher mica content either soften stably with increasing strain following a broad stress peak (transitional response; Figs. 6b & e) or exhibit nearly steady-strength response associated with distributed deformation within localized ductile shear zones (ductile-shear response; Figs. 6c & f). Yield stresses (defined as the differential stress at the onset of inelastic deformation) and ultimate strengths of the strongest and weakest of the rocks tested vary by more than a factor of 4 in both $x45z$ and z sample orientations (Table 3), consistent with the results of previous studies (Fig. 1a). In both orientations, post-softening flow stresses of transitional samples are comparable to flow strengths of samples that deformed by ductile shear.

Effect of mica content

Peak differential stresses (or σ_d at 5% axial strain for samples that exhibited steady-strength behavior) vary as a function of bulk mica content for samples shortened in the z (Fig. 7a) and $x45z$ (Fig. 7b) orientations. Results for both sets of experiments reveal a general reduction in strength with increasing bulk mica content, as well as an increased tendency towards ductile shear deformation. However, the location and sharpness of boundaries between the fields of brittle, transitional and ductile shear differ with orientation. Bulk strengths of samples tested in the z orientation decrease continuously with increasing mica content, with the most dramatic strength reduction occurring within the field of brittle fracture, which persists to mica contents of ~30 vol %. Strengths continue to drop with mica contents beyond 30%, gradually approaching that of the most micaceous rock tested (biotite schist; 75 vol % biotite), and a transition to steady-strength shear occurs for samples containing ~50% mica.

Samples shortened at 45° to foliation (orientation $x45z$) show a similar, though less systematic, trend of decreasing strength and increasing ductility with increasing mica content. Samples with <20% mica by volume are the strongest of those tested in this orientation and exhibit brittle behavior. The fields of transitional and ductile shear deformation overlap considerably at higher mica contents, although rocks containing >40 vol % mica generally deform stably by ductile shear. Data within each of these fields show considerable scatter and rocks of comparable mica content may vary in strength by factors as large as three.

Mechanical anisotropy

Strengths were measured for both the z and $x45z$ orientations for six of the starting materials, and used to determine anisotropy coefficients $[\sigma_d(z)/\sigma_d(x45z)]$ (Fig. 8). The range of anisotropy coefficients determined in this study is comparable to that shown by results published previously by other workers (Fig. 1b). With the exception of the Sandy Formation schist (with a coefficient of 3.2), however, rock types that we tested show strength contrasts of less than a factor of 2. The coefficients shown in Fig. 8 may underestimate the maximum strength anisotropy for some of the rocks tested, since some foliated rocks may be weakest shortened at ~30° to foliation (e.g. Donath 1961, 1964, McLamore & Gray 1967). However, published results for other foliated rocks suggest that the ratio of maximum to minimum strength does not differ from the anisotropy coefficient defined here by more than 20%.

MICROSTRUCTURAL OBSERVATIONS

Microstructures within all faults and shear zones reveal that deformation was accommodated by a combination of cataclastic and crystal-plastic (i.e. semi-brittle) mechanisms. At the test conditions chosen for this study, micas deform readily by basal glide and kinking, as well as frictional sliding along cleavage, except when their {001} planes are oriented nearly perpendicular to σ_1. Quartz, feldspar and all other abundant phases (except calcite, which is present in small amounts as multigranular inclusions in some Appalachian Drill Hole cores), deformed solely by microcracking in all experiments. The bulk behavior of these polyphase aggregates is influenced by the degree to which strains can be accommodated by deformation of micas or require fracture through framework silicate domains. The degree to which micas take up strain depends critically upon the angle β between σ_1 and the foliation plane, as well as the concentration of micas and their spatial arrangements and orientational distributions.

In the following, we describe the intragranular deformation mechanisms that operate within individual mica grains, and show how differences in the geometries and characteristic spacing of micas in different rocks lead to variations in the mechanisms and modes of strain localization.

Mica deformation microstructures

Microstructures developed within individual mica grains are similar to those reported in previous studies

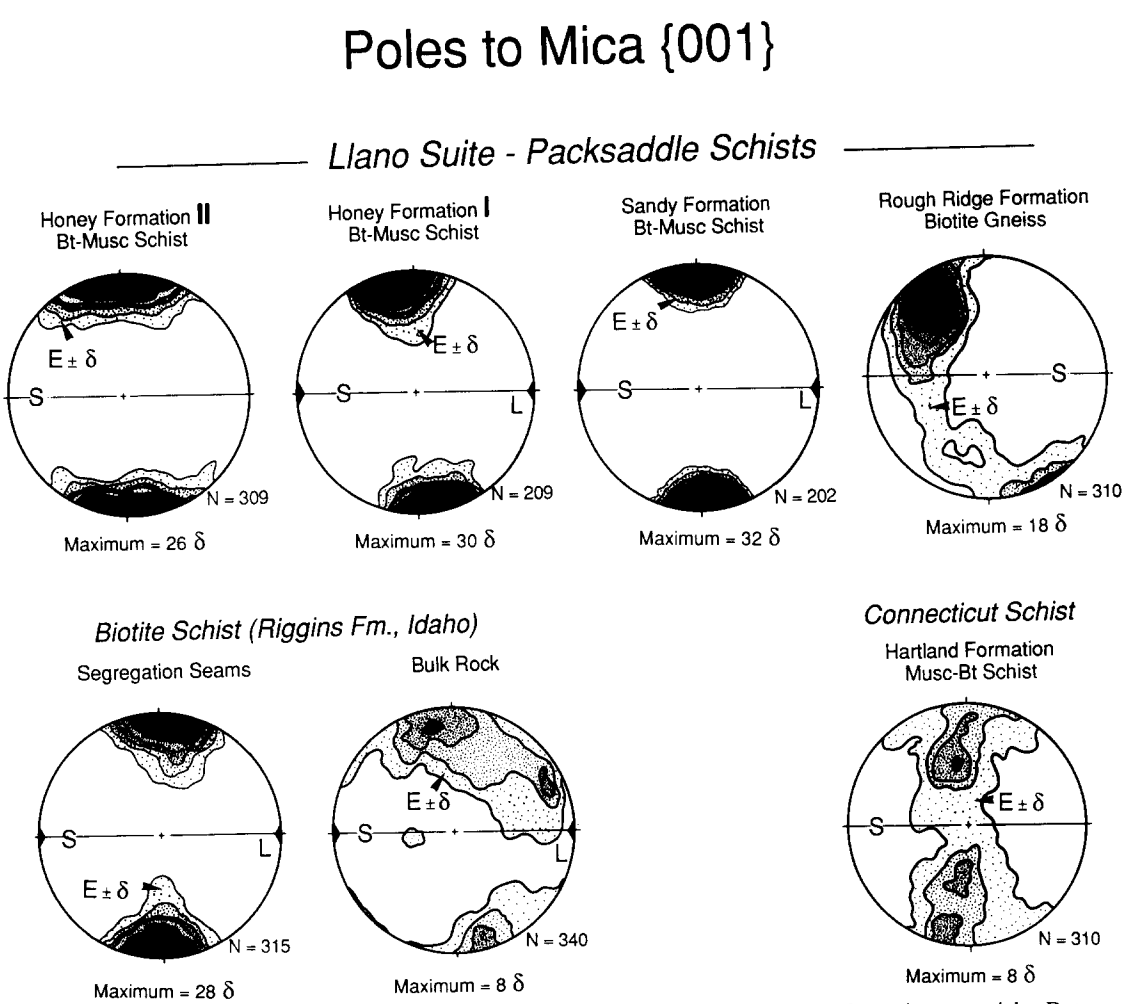

Fig. 5. Equal-area stereographic projections of poles to mica {001} planes in selected starting materials. Data are contoured according to the method of Kamb (1959) in terms of E, the expected density of poles for a randomly distributed pattern, and δ, the first standard deviation from E. Contours are spaced at 2δ intervals, and the maximum contour and number of grain measurements, N, are shown beside each plot. In most samples, mica {001} planes define strong maxima perpendicular to mesoscopic foliation (S). Some show weak partial girdle distributions about lineations (L), as well. However, poles to mica {001} planes may also be more widely distributed (e.g. Hartland Formation), or preferentially aligned to shallow (Honey Formation I) or intermediate angles (Rough Ridge Formation) to S, defined by compositional layering.

(e.g. Bell *et al.* 1986, Shea & Kronenberg 1992), and indicate that dislocation glide and fine-scale microkinking were the dominant mica deformation mechanisms in all rock types tested. Glide of isolated basal dislocation (Fig. 9a) accommodates the low intragranular strains that develop at distances from discrete shear zones, and by inference, during the early stages of deformation within the shear zones. With increased deformation, dislocations organize by glide (Christoffersen & Kronenberg 1993) into planar walls at high angles to (001)(Fig. 9b). As the densities of dislocations within walls increase, small (<0.2 μm wide) cleavage-parallel cracks form, spaced along the low-angle boundaries. These cracks appear to form in response to local stress fields of irregularly stacked dislocations (Christoffersen & Kronenberg 1993), and open to accommodate the formation of high-angle kink-band boundaries (Bell *et al.* 1986). Highly deformed mica grains commonly contain high densities of well developed kink bands, which may intersect and overlap in complex patterns. Individual kink bands range in width from <0.1 to 10 μm (Figs. 9c & d); their boundaries appear sharply defined at the optical scale, but at the TEM scale are seen to contain prominent open voids.

Inter-grain interactions

Differences in the microstructures developed within the interiors of faults and shear zones of different samples can be attributed, with few exceptions, to variations in the initial spacing and concentration of mica and non-mica phases. In low mica content samples, individual mica grains or multigranular mica clusters are isolated in a matrix of stronger silicates, and significant inelastic strains cannot be accommodated without extensive microcracking of the predominantly quartzofeldspathic framework. At the confining pressure of the experiments, microcracking of resistant mica-free regions (or bridges) leads to the development of throughgoing shear fractures at low axial strains. Intragranular microcracks and longer cataclastic shear planes within the strong silicates show close geometrical relationships with inclined mica grains and clusters (Figs. 10a & b). These relationships suggest that microcracks are prefer-

Table 3. Mechanical results for mica-rich rocks

Experiment number	Formation/ source	Stress–strain response*	σ_y† (MPa)	ε_y‡ (%)	σ_{pk}§ (MPa)	ε_{pk}‖ (%)	$\sigma_{2\%}$¶ (MPa)	$\sigma_{5\%}$** (MPa)	Total % ε	Shear zone angle††
*z*45*z* orientation										
A2-095-01	DH 2—29 m	DS	210	0.93	—	—	261	256	8.7	33, 45
A2-143-01	DH 2—43.6 m	B	451	1.41	464	1.52	—	—	1.6	34
A2-277-01	DH 2—84.4 m	DS	261	1.02	—	—	326	322	6.9	45‡‡
A2-416-01.S	DH 2—126.8 m	B	246	0.65	260	0.78	—	—	0.8	37
A4-248-01	DH 4—74.6 m	T	182	0.57	206	0.82	—	—	1.5	38
A4-248-02	DH 4—74.6 m	DS	150	0.61	—	—	165	173	5.5	45‡‡
A4-559-01	DH 4—170.4 m	B	421	1.27	488	1.97	—	—	2.0	30
A4-768-01.S	DH 4—234.1 m	DS	254	0.85	—	—	286	280	9.2	29, 45
A4-793-01	DH 4—241.8 m	T	324	1.18	366	2.01	—	—	2.5	45
BG-S01	Rough Ridge	T	335	0.89	403	2.15	—	330	5.2	30
BS-S01	Riggins	DS	175	0.55	—	—	271	260	7.5	45‡‡
CLS-S1	Honey II	DS	340	1.87	—	—	354	402	7.9	45‡‡
DMS-S01	Sandy	DS	99	0.63	—	—	163	179	9.9	45‡‡
MS-S01	Honey I	T	208	0.87	353	2.38	—	322	7.6	32
z orientation										
A2-416-03.Z	DH 2—126.8 m	B	321	1.09	338	1.66	—	—	1.7	30
A4-768-02.Z	DH 4—234.1 m	T	350	1.05	434	1.85	432	360	6.7	47
BG-Z01	Rough Ridge	T	299	1.31	393	2.87	—	341	6.8	38
BG-Z02	Rough Ridge	T	311	1.26	408	2.58	—	—	3.0	39
BS-Z07	Riggins	DS	177	0.40	—	—	257	241	6.9	42
CLS-Z02	Honey II	B	475	1.70	669	3.68	—	—	3.7	29
DMS-Z01	Sandy	B	479	1.64	575	1.97	—	—	2.0	50
H770-Z01	Hartland	DS	263	1.04	—	—	330	318	8.8	43
MS-Z01	Honey I	T	273	1.07	368	2.15	—	—	2.9	38

*B = brittle; T = transitional; DS = ductile shear; see text for details.
†Differential stress ($\sigma_1 - \sigma_3$) at the inelastic yield point (onset of non-linearity in the stress–strain curve).
‡Axial strain ε at the inelastic yield point.
§Peak differential stress. Data only reported for experiments in which brittle fracture or strain softening occurred.
‖Axial strain at the peak differential stress.
¶Differential stress at 2% axial strain. Data not reported for experiments in which brittle fracture or strain softening occurred.
**Differential stress at 5% axial strain.
††As measured from thin sections prepared parallel to cylinder axis and perpendicular to shear zones.
‡‡Multiple shear zones formed parallel to *S*, within mica segregations.

entially initiated at stress concentrations generated in the vicinity of micas that undergo slip and kinking, much as reported by Gottschalk *et al.* (1990). Micas inclined to σ_1 may act either as isolated shear flaws or as interacting flaws, depending upon the overlap and spacing of neighboring micas relative to their lengths. Evidence for crack initiation is also found, though with less frequency, in *z* orientation samples (shortened normal to foliation) associated with a subset of grains inclined at low to moderate angles to *S*.

With increasing mica concentration, the interconnections across stronger phases are reduced in dimension and strains within brittle–plastic shear zones are accommodated by simultaneous slip and kinking in micas and microcracking in the other phases (Fig. 10c). At large shear strains, microcracking leads to cataclastic grain size reduction in the stronger silicates and the redistribution of phases along shear fractures. In samples of sufficiently high mica content, axially-imposed shortening may be accommodated largely by distributed slip and kinking of interconnected micas within throughgoing, mm-wide shear zones (Fig. 10d). In these samples, stronger silicates (quartz, feldspar, amphibole, epidote) constitute isolated, strong inclusions that remain relatively undeformed within shear zone interiors.

Sample-scale modes of deformation

While a single mechanism of strain localization might be implied by the observation that shear zones developed in all deformed samples, microstructural observations suggest that a variety of mechanisms lead to the nucleation and growth of faults and shear zones in the group of rocks we tested. A series of deformation regimes can be identified for samples shortened in both the *x*45*z* and *z* orientations based upon the microstructures that developed. Three classes of deformation mode can be recognized that coincide with the regimes of brittle, transitional and ductile shear response defined on the basis of mechanical results. However, boundaries between these regimes are gradational, and transitional samples cannot be distinguished from either brittle or ductile samples on the basis of microstructure alone. Photomicrograph mosaics that illustrate the microstructural characteristics of these three modes of deformation in samples shortened normal to *S* (*z* orientation) and at 45° to *S* (*x*45*z* orientation) are shown in Figs. 11 and 12, respectively, and described below.

z orientation. A single discrete fracture developed in each of the brittle samples shortened in the *z* orientation

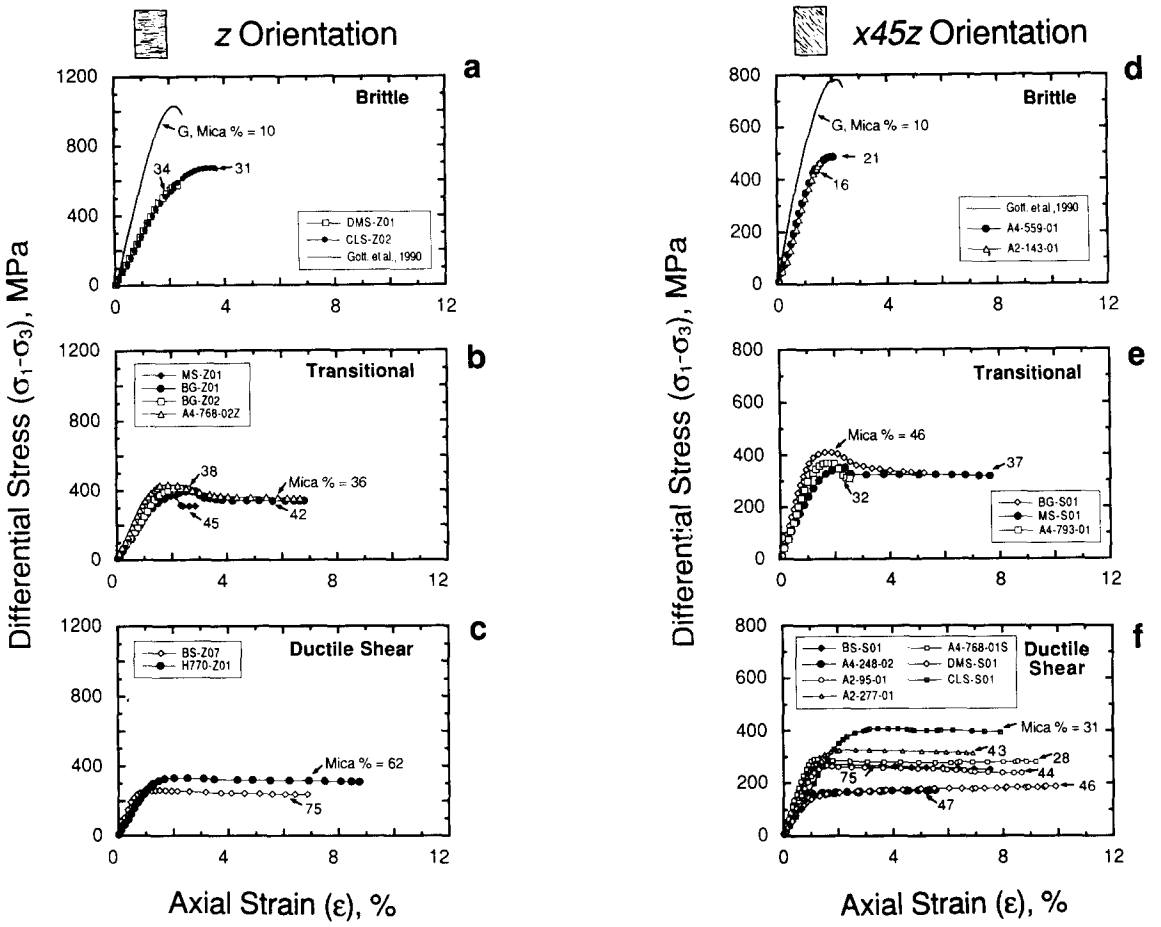

Fig. 6. Differential stress ($\sigma_1 - \sigma_3$) vs axial strain (ε) data for samples shortened at (a–c) 90° to foliation (orientation z) and (d–f) 45° to foliation (orientation $x45z$). Mica contents (in vol %) are shown for each sample, and experiment numbers correspond to those shown in Table 2. Mechanical response for each sample can be classified as either (a & d) brittle (sudden stress drops accompany strain localization), (b & e) transitional (samples soften stably with strain) or (c & f) ductile shear (shear zone localization occurs at steady differential stresses). Data points labeled with a 'G' are from Gottschalk *et al.* (1990).

(Fig. 11). Fracture surfaces are irregular, and link transgranular microcracks (oriented nearly parallel to σ_1) and higher angle intergranular cracks that follow grain boundaries and cleavage planes within mica and feldspar grains. Although micas within the fracture path are commonly deformed by kinking and slip (even when inclined at 70–90° to the compression axis), little evidence for mica plasticity can be detected away from the fracture surface. Fracture appears to have been accomplished largely by the nucleation, propagation, and coalescence of microcracks in phases other than micas, by the same processes that have been documented in experimentally deformed granites (Wawersik & Brace 1971, Peng & Johnson 1972, Tapponier & Brace 1976, Tullis & Yund 1977, Wong 1982).

The geometries of shear fractures appear to be influenced by the degree to which micas are dispersed or segregated within samples. Where micas are evenly dispersed or concentrated in thin, irregular films parallel to S, fractures are nearly planar and inclined at low angles to σ_1 with no apparent geometrical relationship to mica grains. In samples containing thicker mica interlayers, fractures are inclined at higher angles to σ_1 with a distinctly stepped geometry (Fig. 11a). These fractures consist of alternating segments that cut steeply across quartzo-feldspathic domains, and run along mica seams (nearly-parallel to S) for short distances (typically <0.5 mm).

Brittle–plastic shear zones of finite thickness developed within transitional (Fig. 11b) and ductile (Fig. 11c) samples. In both deformation regimes shear zones locally overprint the original metamorphic texture. Displacements across these shear zones are accommodated by distributed slip and micro-kinking in the micas and grain-scale cataclasis of all phases. Within transitional shear zones (Fig. 11b), significant redistribution of micas and other phases occurs. In the early stages of deformation, micas are sheared along discrete cataclastic shear planes and intermixed with surrounding phases. The mechanical redistribution mechanism appears to operate by processes similar to those proposed by Jordan (1987) for uniformly dispersed aggregates with a weak plastic component and a stronger brittle or semi-brittle phase. With increasing strain, crude fine-scale compositional foliations that are distinct from the original metamorphic foliation develop at low angles to the shear zone boundaries, and are most pronounced in areas where shear zones transect relict domains of low initial mica content.

Ductile shear zones are morphologically similar to

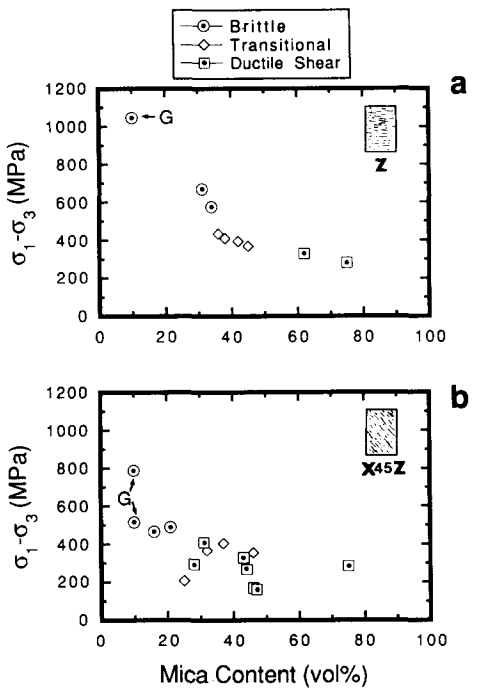

Fig. 7. Peak differential stresses (or stresses at 5% strain for samples showing ductile shear response) as a function of bulk mica content (by vol %) for (a) samples shortened at 90° (orientation *z*) to *S* and (b) 45° (orientation *x*45*z*) to *S*. The *z* orientation data show a clear trend of decreasing strength and increasing ductility with increasing mica content, while results for *x*45*z* samples show a similar, but less systematic, trend. Data points labeled with a 'G' are from Gottschalk *et al.* (1990).

those developed in the transitional deformation field, but strains are accommodated within wider (up to several mm wide), irregular zones and accommodated almost exclusively by slip and intense micro-kinking within a network of interconnected micas (Fig. 11c). Stronger phases are fractured but remain as isolated clasts.

x45z orientation. Three distinct modes of deformation are also recognized in *x*45*z* samples. In this orientation, however, strains localize parallel or at shallow angles to *S*, typically within mica-rich horizons. The transition from brittle faulting to ductile shear is closely associated

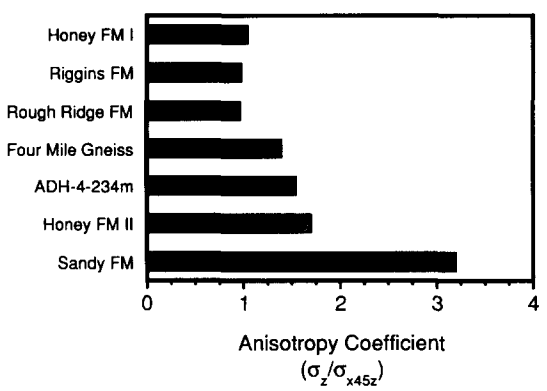

Fig. 8. Anisotropy coefficients (σ_z/σ_{x45z}) of samples deformed in this study for starting materials shortened in both the *z* and *x*45*z* orientations, respectively. With the exception of the Sandy Formation schist, the strengths of many foliated rocks we tested varied by less than a factor of 2 when shortened at 45° and 90° to *S*. Data for Four Mile gneiss are from Gottschalk *et al.* (1990).

with a decrease in the dimension and number of resistant quartzo-feldspathic bridges that must be broken in order to localize strains. Compression of samples in this orientation leads to significantly less mechanical redistribution of phases.

Single, discrete fractures form at shallow angles to *S* (and closer to σ_1) in brittle samples. Fracture geometries appear to be influenced significantly by the spatial arrangement of mica grains and clusters (Fig. 12a), and geometries are remarkably similar to those Gottschalk *et al.* (1990) described in equivalently oriented samples of gneiss. Fracture surfaces have a stepped geometry with segments that are parallel to *S* as they follow (001) cleavage planes of inclined mica grains, and segments at angles ranging from 5° to 20° to the σ_1-compression direction where they cut across intervening quartzo-feldspathic bridges. Microcrack densities are distributed heterogeneously along the length of the fracture zone. Few microcracks are present in quartz and feldspar grains adjacent to elongate mica clusters, while high densities of low-angle extension microcracks transect mica-free bridges nearly parallel to the direction of applied shortening. These microcracks appear to have been generated near the tips of inclined micas, and commonly link neighboring mica clusters spaced in en échelon configurations. The sense of step (as defined by Segall & Pollard 1980) between neighboring micas along the fracture is nearly everywhere one that leads to enhanced tensile stresses in the region of overlap.

Microstructures in transitional samples reveal brittle–plastic interactions similar to those observed in samples that deformed by brittle failure (Fig. 12b), and the transition from brittle failure marked by abrupt stress drops to gradual strain-softening is associated with an increase in length or decrease in spacing of mica clusters within the shear zone path. Most mica clusters deform internally by slip and kinking. As in brittle samples, sets of low-angle microcracks within quartz and feldspars emanate near the ends of adjacent mica clusters. Microcracks are also common along the interfaces between kinked micas and neighboring grains.

One or several ductile shear zones may be developed parallel to *S* within samples that deform at constant flow stress. Shear zone microstructures (Fig. 12c) are similar to those that developed in *z* orientation samples, with strains accommodated primarily by slip and kinking within interconnected micas. In *x*45*z* samples, however, ductile shear zones occur in samples with a range of bulk mica contents, and displacements are localized within nearly-continuous to continuous mica segregations of varying width and tortuosity.

Despite the predominance of kink bands and extreme undulatory extinction within the micas, quartz and feldspar grains within the interior of most ductile shear zones contain abundant microcracks. Microcrack densities appear to be related to the thickness and spatial distribution of mica segregations, as revealed clearly by microstructural maps constructed from shear zone interiors of samples with different mica seam geometries. In samples with distinct mica interlayers (Fig. 13a), high

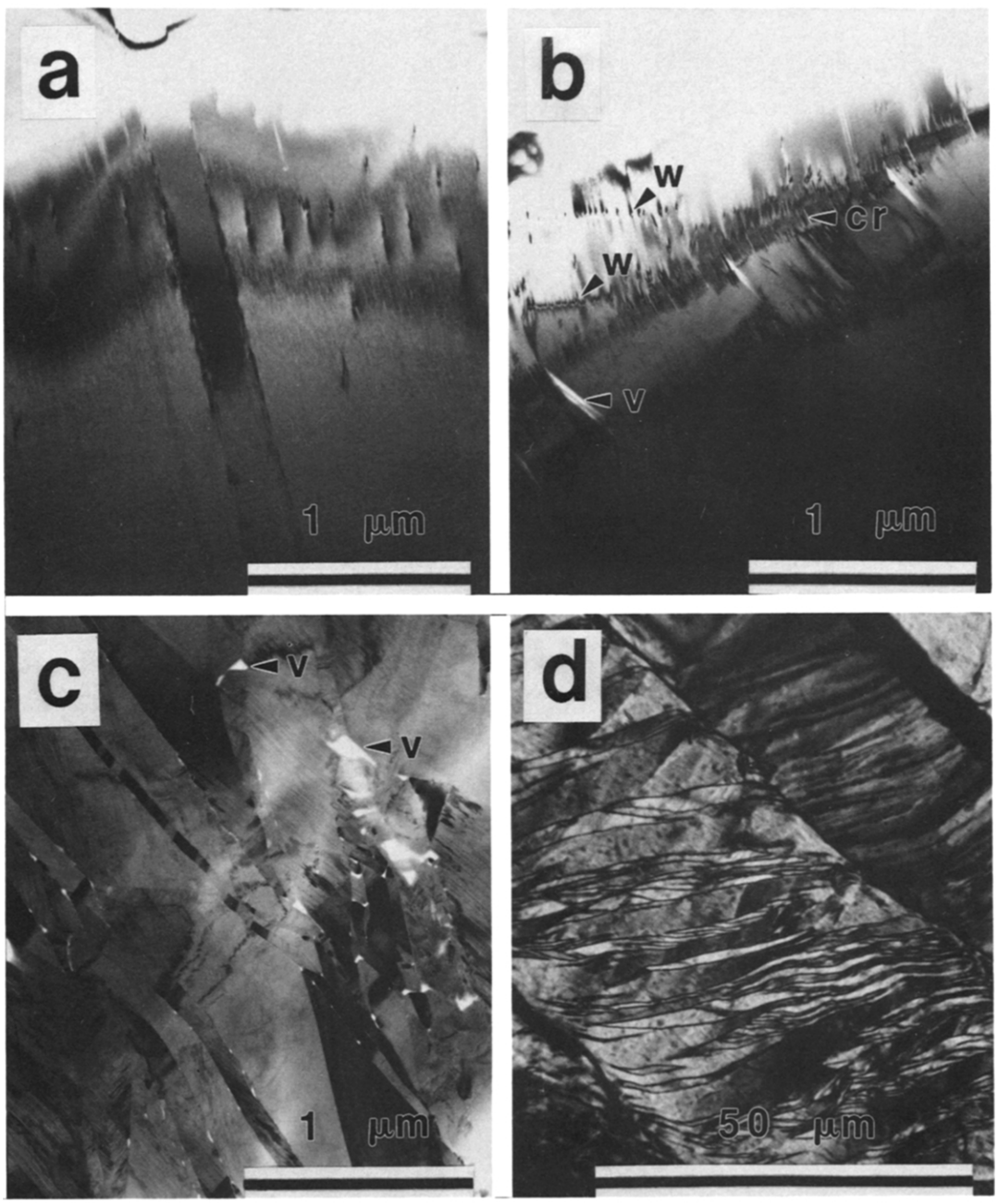

Fig. 9. Grain-scale microstructures of deformed micas from Riggins Formation biotite schist (sample BS-S1). (a–c) Bright field TEM micrographs. (a) Isolated basal dislocations developed in unkinked grain. (b) Organized dislocation walls (w) within biotite grains, associated with early stages of kink band development. Fine-scale cleavage cracks (cr) and voids (v) form along boundaries with densely spaced dislocations. (c) Complex overlapping kink bands within highly deformed biotite grain. Sharply defined kink band boundaries no longer appear as dislocation walls and open, sub-optical voids (v) are common. (d) Optical micrograph (crossed polars) of ultra-thin section, showing array of larger-scale kink bands. Voids cannot be detected at optical magnifications, although the sharp nature of boundaries may result from light scattering from closely spaced, fine-scale voids.

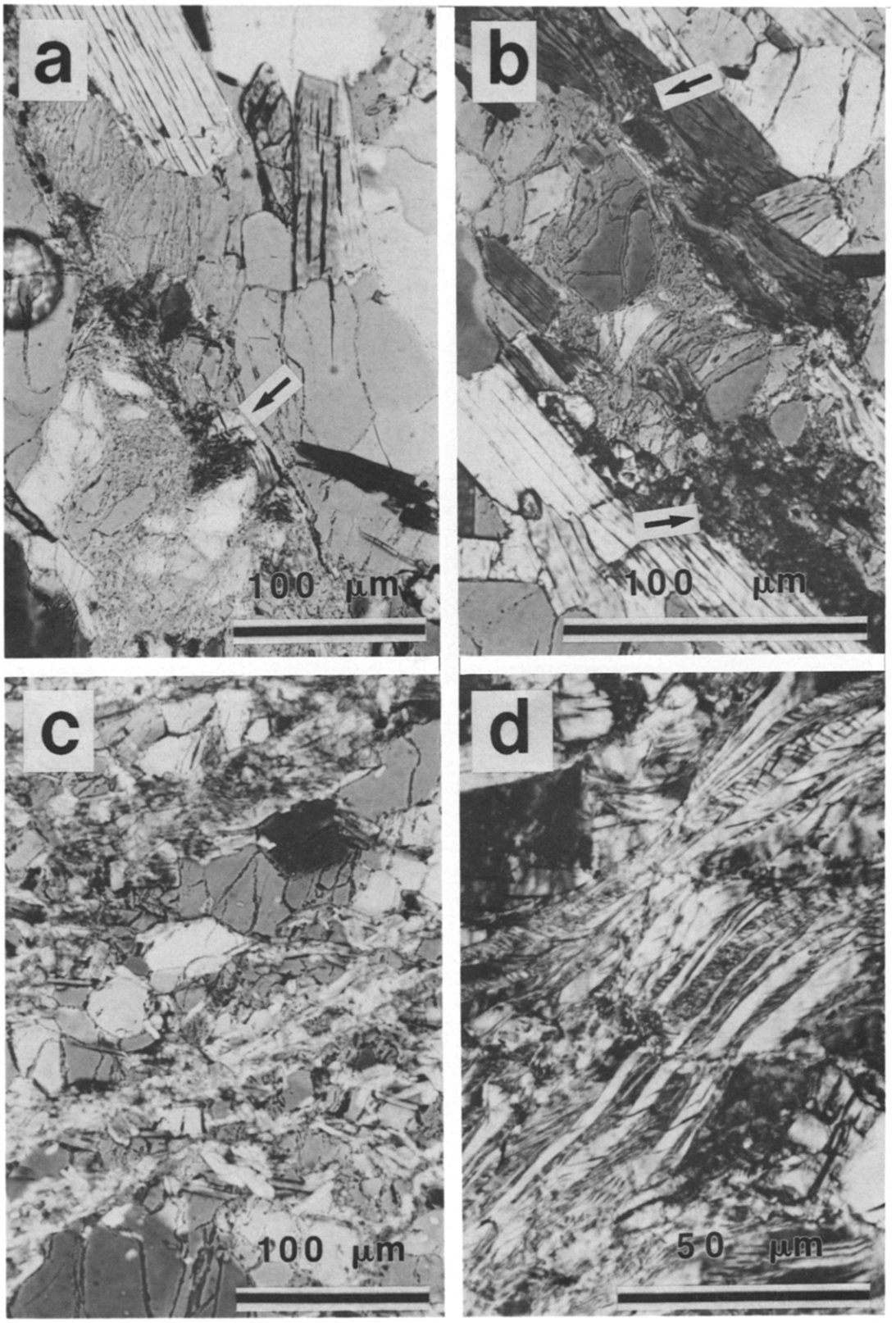

Fig. 10. High-magnification optical micrographs (crossed-polarized light) showing deformation microstructures in micas and neighboring phases in shear zones of varying mica content. The compression axis is shown vertical in each micrograph. (a) Dense sets of low-angle microcracks associated with the tips of mica grains. Intragranular microkink bands (MKBs) only develop within zones of intense comminution along the principal fracture surface (arrow). Sample A4-559-1 deformed in the $x45z$ orientation. (b) Dense microcrack networks form in the overlap region between closely spaced and intensely kinked mica (arrows). Sample A4-248-1 deformed in the $x45z$ orientation. (c) Microcracking persists in shear zones that contain a higher proportion of mica, although a large percentage of total strain is taken up by slip and kinking in micas. Sample CLS-S1 deformed in the $x45z$ orientation. (d) In rocks in which micas occur as interconnected networks across samples along planes of high resolved shear stress, strains are accommodated largely by the development of dense sets of MKBs, which pile up and give rise to complex deformed regions showing many generations of kink bands. Sample H770-Z1 deformed in the z orientation.

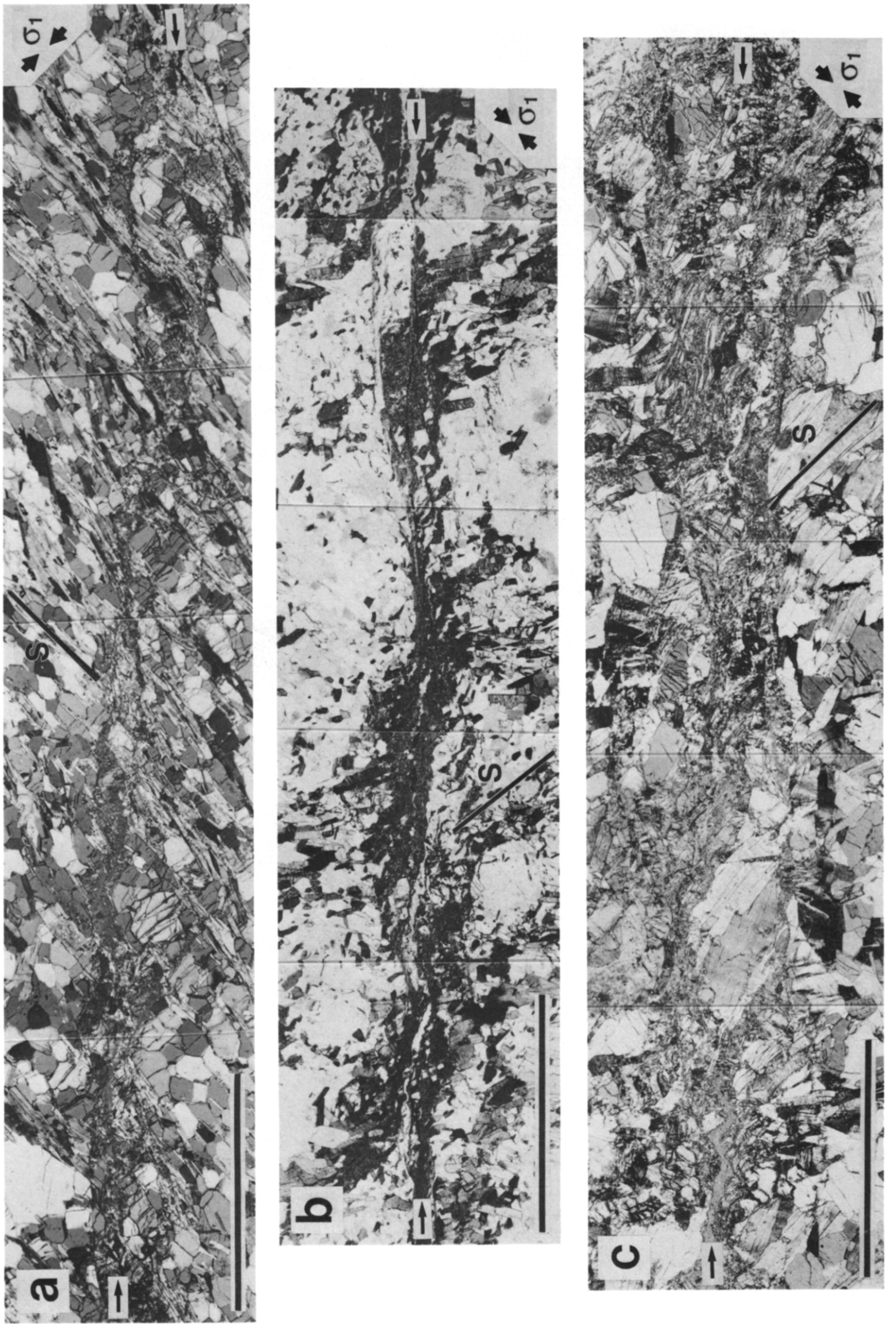

Fig. 11. Photomicrograph mosaics of shear zones that developed in z orientation samples showing (a) brittle, (b) transitional and (c) ductile shear response. Foliation (*S*) and compression directions are shown, and small black arrows indicate the average shear zone trends in each mosaic. Scale bars = 1 mm in all micrographs. (a) Brittle shear zone in sample DMS-Z1 (crossed polars) consists of a highly comminuted central zone surrounded by a wider region containing high densities of microcracks. Microcrack densities are highest where the throughgoing fracture transects quartzo-feldspathic bridges. (b) Transitional shear zone in sample BG-Z1 (plane polars). Micas have been sheared along discrete cataclastic planes within regions of initially low mica concentration. (c) Ductile shear zone in sample H770-Z1 (crossed polars). Deformation is concentrated within a diffuse zone >1 mm wide, and is accommodated largely by slip and grain-scale micro-kinking of interconnected micas.

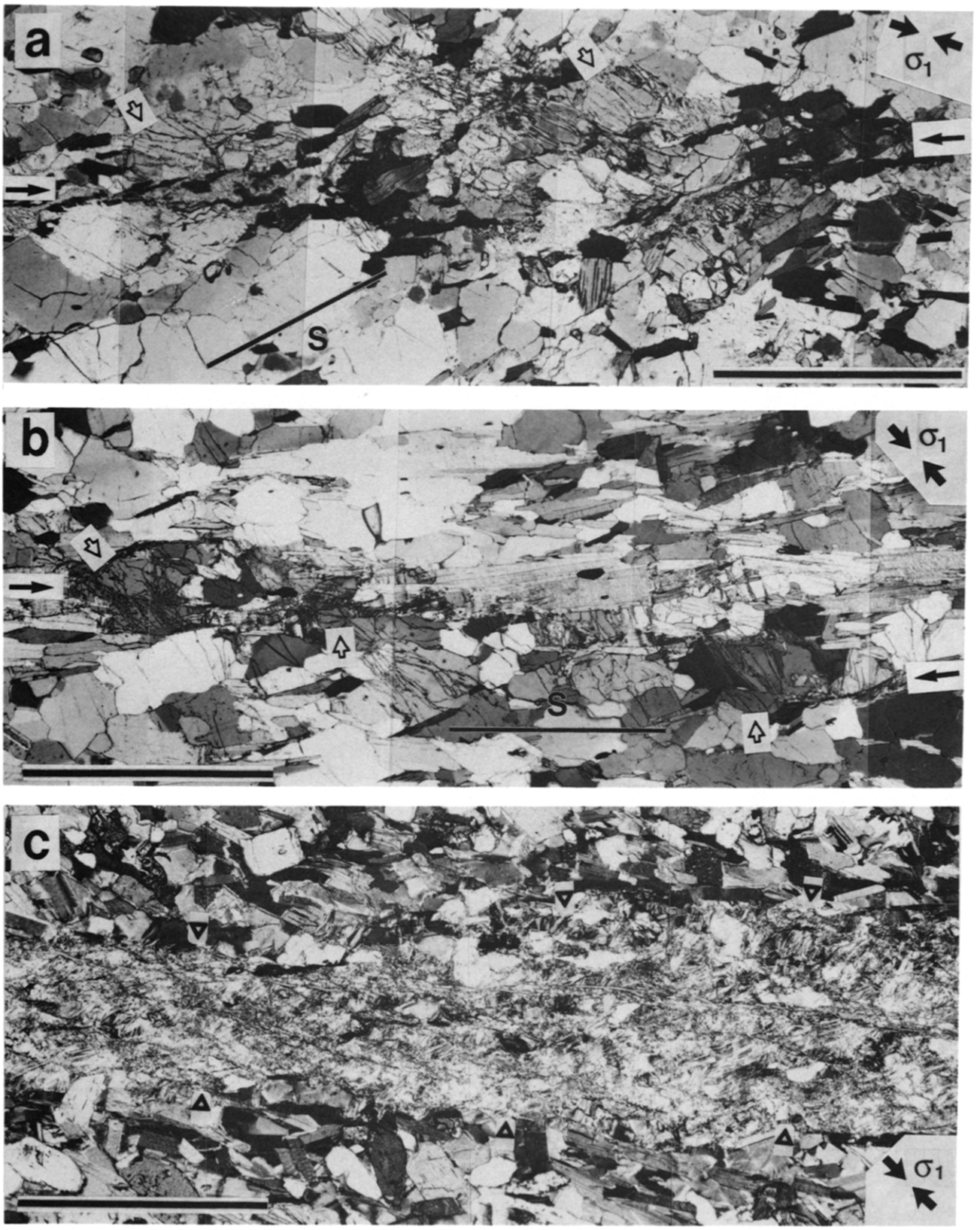

Fig. 12. Photomicrograph mosaics of shear zones that developed in $x45z$-orientation samples that showed (a) brittle, (b) transitional and (c) ductile shear response. Foliation (S) and σ_1-compression directions are shown, and small black arrows indicate the average shear zone trends. All scale bars = 1 mm. (a) Brittle fracture (inclined at ~15° to S) with right-lateral displacement in sample A4-559-1 (plane polars). Low angle microcracks in resistant quartzo-feldspathic bridges (open arrows) connect multigranular mica clusters spaced in en échelon configurations. (b) Shear zone and foliation traces coincide more closely in transitional sample (sample A4-248-1, crossed polars). (c) Strains are concentrated into relatively wide brittle–plastic shear zones in samples with distinct mica seams. Slip and kinking in micas is accompanied by only minor microcracking in the surrounding silicates (sample BS-S1, crossed polars).

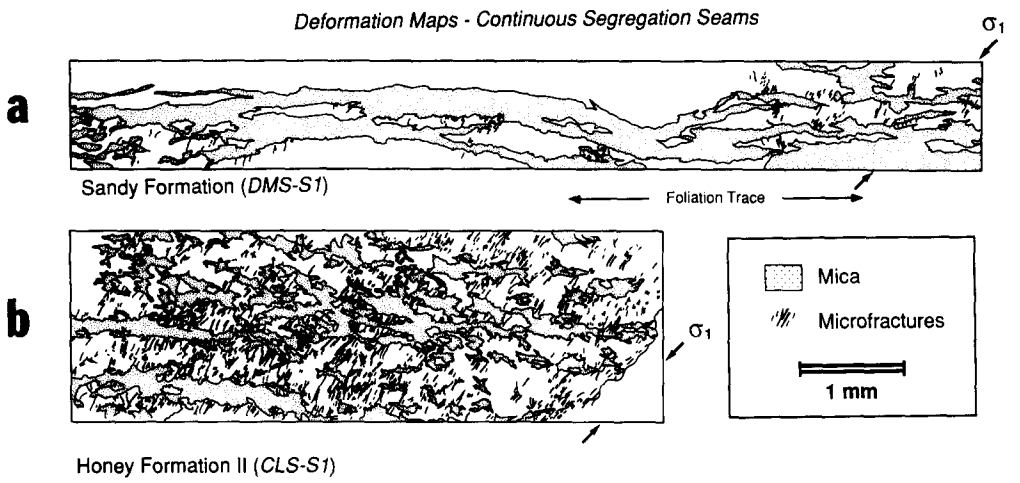

Fig. 13. Microstructural maps of ductile shear zones that developed in samples (a) DMS-S1 and (b) CLS-S1, shortened at 45° to S ($x45z$ orientation), showing the geometrical relationships between microcracks and discrete mica segregations. Strains are localized, and accommodated largely by distributed slip and kinking of micas. In phases other than micas, only limited microcracking occurs in schists that contained thick, nearly planar mica seams (a), except where individual interlayers pinch out. High densities of distributed, low angle microcracks developed within shear zones that localized along narrow, anastamosing mica films (b).

microcrack densities occur only in isolated quartzo-feldspathic clasts, or where prominent mica layers are observed to 'pinch-out' and displacements were required to be transferred to adjacent seams. Relatively uniform, high densities of microcracks are present in samples with narrow (<<1 mm wide), anastamosing mica films (Fig. 13b).

Influence of fabric

The gradual transition from brittle to ductile shear response in both $x45z$ and z orientation samples appears to be associated most directly with variations in the concentration of micas along planes of high resolved shear stress. In samples shortened normal to foliation (z orientation), mica contents along high shear stress planes are similar to bulk sample concentrations, since large numbers of distinct, mm-scale heterogeneities (e.g. mica clusters, lenses or seams) are transected. This observation may explain the systematic variation of strength, mechanical response, and mode of deformation with mica content in z orientation samples.

In contrast, results for $x45z$ orientation samples (shortened at 45° to foliation) show only a crude correlation with bulk mica content. For samples of this orientation, mica lenses and seams are inclined in high shear stress orientations, and deformation tends to localize within weak, mica-rich horizons. Relatively ductile response can occur for samples containing small amounts of mica, provided micas are strongly segregated and form continuous planar zones. The mechanical properties of $x45z$ oriented samples are expected to correlate directly with differences in texture and composition within these critical domains.

Microstructural observations suggest that ductile shear is favored over brittle fracture with increases in the length and contiguity of multigranular mica clusters along planes of high shear stress. We therefore attempted to characterize these textural elements and identify the extent to which they influence mechanical response (and corresponding modes of deformation) by measuring three additional starting material characteristics in $x45z$ samples:

(1) linear mica continuity (LMC), defined as the percentage of mica intersected along a single, arbitrary straight-line traverse across a sample;

(2) multigranular mica cluster lengths (L_c) and widths (W_c);

(3) dimensions of quartzo-feldspathic bridges (L_b) separating neighboring mica clusters.

Linear mica continuity (LMC) *measurements* provide a means of characterizing averaged compositions within localized zones that may not necessarily be representative of the bulk material. We measured LMC by taking point counts on 0.1 mm intervals along closely-spaced lines oriented parallel to shear zone traces in all $x45z$ oriented samples. Approximately 140 counts were obtained along each traverse and at least five measurements were made for each sample. Shear zones tend to nucleate along zones of high LMC, and we therefore made measurements along selected traces within shear zone interiors. Although minor mechanical redistribution of phases occurred in these zones, LMC values determined along shear zones are not distinguishable statistically from those obtained along other high contiguity planes. The maximum linear mica continuity (LMC_{max}) for each sample is given in Table 4.

The dimensions of *multigranular mica clusters* and intervening quartzo-feldspathic bridges were measured for samples that lack a continuous network of interconnected micas (i.e. segregations whose lengths are shorter than sample diameters; Table 1 and Fig. 3). Many clusters have highly irregular geometries; measured lengths (L_c) are those of the longest line segment that can be drawn to connect opposite ends of a cluster, and corresponding widths (W_c) represent the maximum dimension measured normal to the direction of L_c. We measured the dimensions of at least 50 clusters

Table 4. Compositional and textural characteristics of samples deformed at 45° to S

Experiment number	Formation/ source	Total phyllosilicate content	Deformation response*	Maximum linear mica continuity (LMC_{max})†	Multigranular mica cluster dimensions				Quartzo-feldspathic bridge dimensions	
					W_{mean}‡ (mm)	W_{max}‡ (mm)	L_{mean}§ (mm)	L_{max}§ (mm)	L_{mean}‖ (mm)	L_{max}‖ (mm)
A2-095-01	DH 2—29 m	44	DS	62	—	—	—	—	—	—
A2-143-01	DH 2—43.6 m	16	B	18	—	—	—	—	0.32	0.88
A2-277-01	DH 2—84.4 m	44	DS	88	—	—	—	—	—	—
A4-248-01	DH 4—74.6 m	25	T	58	0.20	0.65	0.95	3.31	0.21	0.70
A4-248-02	DH 4—74.6 m	48	DS	93	0.29	3.28	1.63	12.53	0.18	0.32
A4-559-01	DH 4—170.4 m	21	B	34	0.11	0.47	0.29	0.86	0.31	0.80
A4-768-01.S	DH 4—234.1 m	28	DS	63	0.16	0.54	1.00	5.57	0.28	0.58
A4-793-01	DH 4—241.8 m	33	T	54	0.23	1.27	1.02	2.98	0.23	0.34
BG-S01	Rough Ridge	37	T	55	—	—	—	—	—	—
BS-S01	Riggins	76	DS	88	—	—	—	—	—	—
CLS-S1	Honey II	30	DS	45	—	—	—	—	0.21	0.55
DMS-S01	Sandy	46	DS	93	—	—	—	—	0.11	0.22
MS-S01	Honey I	46	T	57	0.032	0.066	0.21	0.59	0.07	0.23
DOE-28	Four Mile gneiss¶	10	B	12	0.14	0.37	0.72	2.06	1.46	4.51

*B = brittle; T = transitional; DS = ductile shear.

†Volume percentage of mica intersected along linear traces parallel to throughgoing faults or shear zones in samples, as determined from ~140 point counts (0.1 mm spacing) per traverse.

‡W_{mean} and W_{max} refer to the average and maximum widths, respectively, of multigranular mica clusters, as described in the text.

§L_{mean} and L_{max} refer to the average and maximum lengths, respectively, of multigranular mica clusters, as described in the text.

‖L_{mean} and L_{max} refer to the average and maximum dimensions, respectively, of resistant quartzo-feldspathic bridges, as described in the text.

¶Sample obtained from study by Gottschalk *et al.* (1990).

in each sample, selecting grains at evenly-spaced intervals along photomicrograph mosaics.

Quartzo-feldspathic bridge dimensions are more difficult to define than the sizes of isolated mica clusters, particularly in those samples with irregularly distributed micas of varying sizes. Gottschalk *et al.* (1990) characterized interaction distances between neighboring biotite grains in gneiss by measuring nearest-neighbor distances (r), normalized by the mean half length (a) of each mica pair. Even for this rock with relatively low bulk mica contents, elastic interactions were important for a significant fraction of grains. Perturbing stress fields are important for a much greater percentage of mica cluster pairs in the higher mica content samples tested in this study. However, we could not tractably measure spacings between all interacting mica cluster pairs, and instead characterized the dimensions of a much smaller number of cracked bridges in deformed samples. As a measure of bridge dimension we define L_b as the average length of a microcracked zone that links kinked micas. These microcracked zones are found between or ahead of the tips of neighboring mica clusters, and ultimately control the morphologies of throughgoing shear zones in $x45z$ samples. Where transgranular microcracks connect the tips of neighboring mica grains (e.g. Figs. 10a & b) or mica clusters, this dimension corresponds to the length of the cracked zone from one tip to the other. For overlapping mica clusters L_b represents the mean crack length in the region of overlap. Mean and maximum values of L_c, W_c and L_b are shown in Table 4.

Bridge and cluster dimensions for individual samples are compared by means of probability plots that show the percentage of clusters (Fig. 14a) and bridges (Fig. 14b) with lengths equal to or smaller than any specified reference length. Length measurements were normalized to sample dimensions by dividing each characteristic dimension by the length of a foliation-parallel transect across samples (~12.6 mm). Median mica cluster lengths (i.e. lengths that correspond to the 50th percentile) for all starting materials that we measured fall within a relatively narrow range and are always less than one-tenth of the length of foliation-parallel transects across individual samples. There are distinct differences, however, in the lengths of the longest clusters in each sample (i.e. clusters whose lengths fall in the 90–100th percentiles) that can be related to differences in mechanical behavior. Samples A4-248-2 and A4-768-1, which exhibited ductile-shear mechanical response, contain a subset of clusters that are longer than the largest clusters measured in brittle and transitional samples. Brittle and transitional samples do not appear to contain clusters with normalized lengths greater than 0.25. Samples in the brittle and transitional deformation regimes cannot be distinguished on the basis of cluster length distributions, however, and strength differences among samples do not correlate directly with differences in the lengths of the largest clusters.

Median and 90th percentile bridge dimensions, L_b, are both greater for those samples that failed by brittle fracture, and strengths in the brittle field do appear to increase with bridge size (Fig. 14b). However, samples that fail by transitional strain-softening and ductile shear cannot be discriminated on the basis of bridge size alone, and the data do not describe a simple strength vs bridge size relationship in these fields.

The inability of either dimension, L_c or L_b, to distinguish all three observed modes of deformation suggests that a combination of microstructural parameters influences the mode of deformation and strength

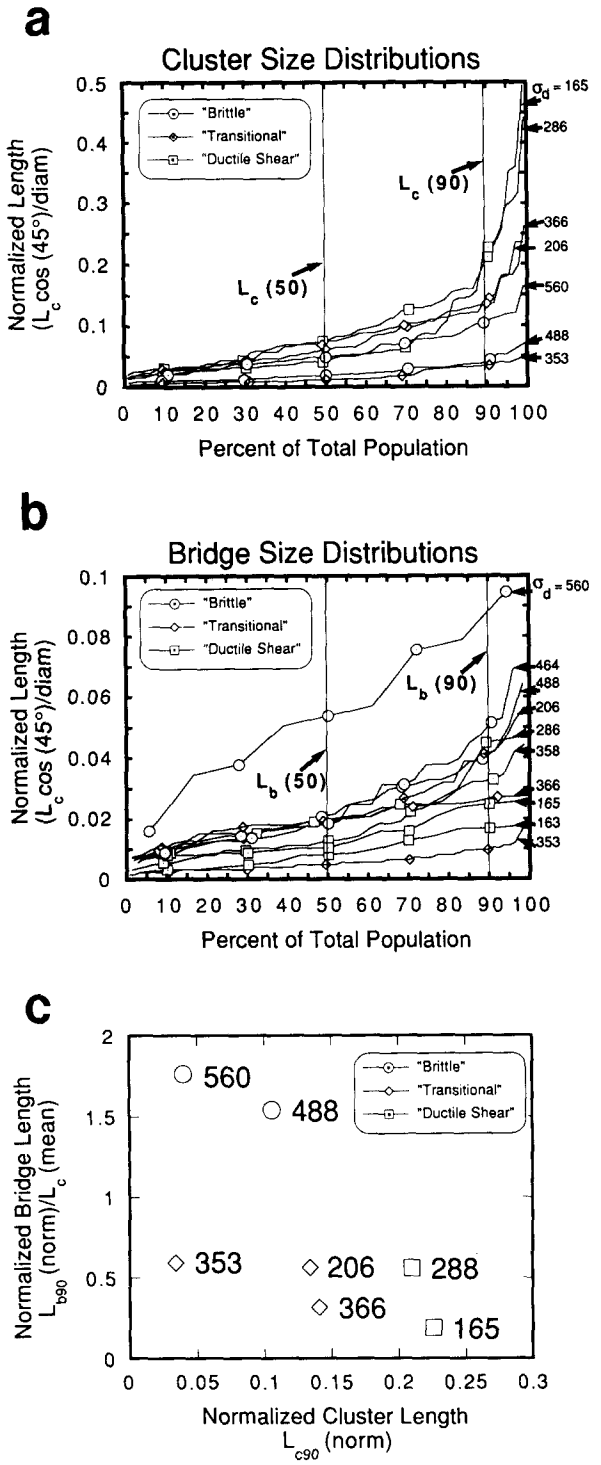

Fig. 14. Mica cluster and quartzo-feldspathic bridge dimensions for deformed $x45z$ samples. (a) Probability plot of length distributions of multigranular clusters for samples that lacked throughgoing mica segregations, normalized to sample size. Peak (or steady-strength) differential stresses are also shown at the right. Although median lengths of mica clusters are similar, dimensions of the longest clusters (i.e. those within the upper 90th percentile) differ markedly among samples. (b) Probability plot of bridge size distributions for deformed samples, normalized to sample size (stresses shown at right). (c) Cross-plot of bridge length L_b at the 90th percentile (normalized by both the sample size and mean cluster length L_c) vs cluster length L_c at the 90th percentile (normalized by sample size). Distinct fields of brittle, transitional and ductile shear response may be identified. Differential stresses measured for these samples show an imperfect trend of increasing strength (to the upper left corner) with reductions in L_c and increases in L_b.

in these rocks. If we plot the 90th percentile bridge dimensions L_b (normalized by both sample dimension and mean cluster length) against 90th percentile normalized cluster length L_c (Fig. 14c), all three modes of deformation may be distinguished, with fields of brittle deformation for small L_c and large L_b, ductile shear for large L_c and small L_b, and transitional response for samples with small to intermediate L_c and L_b. However, within individual fields of deformation response, strengths are not well correlated with these measures of individual cluster and individual bridge dimensions.

Unlike measurements of L_c and L_b, our measurements of LMC_{max} along line traverses within shear zones capture the relative proportions of weak micas and strong quartz and feldspars along potential failure planes. When peak (or steady-strength) differential stresses are plotted as a function of LMC_{max} (Fig. 15), the data for $x45z$ samples define a clear trend of decreasing strength and increasing ductility with increasing LMC. Brittle, fracture-dominated deformation occurs in all samples with LMC_{max} <35%, while ductile-shear response occurs in all samples with LMC_{max} >60%. There is only minor overlap of the fields of transitional and ductile-shear mechanical response in comparison to the overlap of deformation fields exhibited by the plot of differential stress vs bulk mica content (Fig. 7b). Again, while the maximum mica continuity LMC_{max} helps explain the variation in deformation of foliated rocks shortened at 45° to S, strength variations as great as a factor of 2 are nonetheless apparent between samples of comparable maximum mica continuity. The range of strengths at constant LMC is similar to the range defined by strengths of samples with constant bulk mica content (Fig. 7b). Like the combined cross-plot of normalized L_c and L_b measurements (Fig. 14c), LMC measurements appear to be reliable predictors of the relative ductility of samples, but allow only approximate estimates of the relative strengths of different rock types.

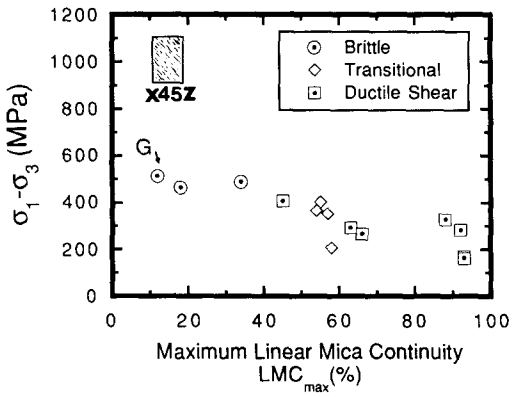

Fig. 15. Peak differential stresses (or stresses at 5% strain for samples showing ductile shear response) plotted as a function of maximum linear mica continuity (LMC_{max}) for samples shortened at 45° to S (orientation $x45z$). The fields of brittle, transitional and ductile shear response appear organized, with brittle and transitional behavior at low values of LMC_{max} and ductile shear at higher values of LMC_{max}; this trend is more systematic than that revealed by bulk mica content (Fig. 7). However, strengths may vary by a factor of 2 for a given value of LMC_{max}.

DISCUSSION

The compressive strengths and mechanical anisotropies of the foliated rocks tested in this study span ranges that are comparable to those reported in previous studies on other foliated rocks tested in the same orientations (Fig. 1). These results reveal the extent to which variations in the concentration, spatial arrangement and preferred orientations of micas can influence the bulk mechanical behavior of polymineralic aggregates composed largely of other, stronger mineral phases. By correlating the mechanical results obtained in this study with petrographic observations of both the starting materials and deformed samples, we have identified specific textural and compositional characteristics of mica-bearing rocks that appear to influence their mechanical response most directly. These variables include bulk mica concentration and preferred orientation, contiguity of micas along planes of high resolved shear stress, and the dimensions of multigranular mica clusters and intervening quartzo-feldspathic bridges. In the following, we consider the extent to which variations in mechanical behavior among samples can be explained by differences in these microstructural parameters, and the degree to which the experimental results obtained here can be applied to problems associated with larger-scale deformations of the same rock types.

Factors that control mechanical response and mode of deformation

Although micas are highly anisotropic, the variation of strength with mica content documented for schists and gneisses deformed in the z and $x45z$ sample orientations (Fig. 7) is in general accord with conceptual models describing the rheologies of two-phase materials made up of strong and much weaker components (Tharp 1983, Jordan 1988, Handy 1990, Tullis *et al.* 1991). With increasing proportions of the weak phase, these models predict a transition in mechanical response from a strong framework-supported composite to a weak matrix-controlled aggregate. For homogeneously distributed phases, the boundary between framework-supported and weak matrix-supported rheologies corresponds to the composition at which a load-bearing framework of strong, stress-supporting grains breaks down throughout the rock mass. The phase configurations in the foliated rocks tested here are considerably more complex and heterogeneous than those considered by the current models, and microstructural observations of the deformed samples (Figs. 10–12) suggest that marked transitions in mechanical response occur once the stress-supporting framework collapses along localized, critically oriented planes. As a result, the strengths of mica-bearing rocks (at the single experimental condition tested) are influenced most directly by the contiguity and orientations of micas along these high shear stress planes, and may not necessarily be predicted readily from the average proportions and strength ratios of the constituent phases. The results of this study suggest that mica content may only be used to predict strengths effectively for sample orientations in which the bulk concentration of micas is similar to the concentration along prospective failure zones inclined at intermediate angles to the σ_1-compression direction, as observed in the z orientation samples. In samples loaded so that large shear stresses are resolved on S (as in $x45z$ orientation samples), predictions of mechanical response cannot be made without considering the effects of isolated networks of weak, interconnected micas that may represent localized zones of weakness.

In z orientation samples, the trend of decreasing strength with increasing bulk mica content (Fig. 7a) is nearly as systematic as that defined by experimental results for homogeneously mixed composites of simpler, more nearly isotropic phases (e.g. halite–anhydrite, Price 1982, Ross *et al.* 1987; halite–calcite, Jordan 1987). In addition, we can identify a transitional deformation regime similar to that observed in these previous studies. Mechanical redistribution of phase components occurs in samples that exhibit stable, strain-softening behavior, leading to increased strain accommodation in the weak phase with increasing shortening. The close correlation between strength and bulk mica content suggests that mica contiguity (which, in this orientation, corresponds closely to bulk mica content) is the most important microstructural parameter controlling strength and stress–strain response. Other factors, including the strength of mica preferred orientations and degree of mica segregation, appear to influence mechanical response much less directly, although the apparent lack of scatter in strengths at constant mica content may be due to the limited size of the data set in this orientation. Given the lack of slip in micas on planes other than {001}, z orientation samples with strong mica preferred orientations parallel to S (i.e. with nearly all {001} planes normal to σ_1) may be expected to have significantly higher strengths than those with more widely distributed grain orientations (in which a large population of grains is oriented favorably for slip and kinking). However, we find no evidence to support this assumption over the range of mica preferred orientations sampled. Further experiments on rocks with similar textures and larger, quantifiable differences in strength of preferred orientation are needed to determine the significance of this variable.

Bulk mica contents do not predict adequately the strengths of $x45z$ oriented samples (Fig. 7b), since the mechanical behavior of samples loaded in this orientation is influenced more directly by the diverse properties of prospective failure planes oriented parallel or at low angles to S. Deformation microstructures in these samples show that strain localization occurs by brittle fracture or distributed flow within brittle–plastic shear zones along planar zones that are rich in micas and serve as flaws or weak links within a sample (Fig. 12). The results of microstructural measurements on these samples (Table 4) have revealed that ductile shear deformation is restricted to samples with multigranular mica clusters that are long relative to sample dimensions

(Fig. 14a). Samples showing brittle, transitional and ductile shear deformation may be adequately distinguished on the basis of their maximum linear mica continuities LMC_{max} (Fig. 15) or from a cross-plot of cluster dimension L_c vs normalized bridge dimension L_b (Fig. 14c). However, samples with similar mica cluster length distributions, quartzo-feldspathic bridge dimensions, and values of LMC_{max} may exhibit strength variations as large as a factor of 2; this result suggests that microstructural elements besides those quantified by these relatively simple parameters must also influence the mechanical response of samples shortened in the $x45z$ orientation.

Within the brittle and transitional deformation fields, variations in strength among samples may depend upon the full distributions of mica and of quartzo-feldspathic bridge dimensions. Several studies have shown that individual mica grains whose basal planes are inclined to σ_1 may generate significant stress concentrations and nucleate cracks near their ends (e.g. Fig. 10), within surrounding phases (Tapponnier & Brace 1976, Wong & Biegel 1985, Gottschalk *et al.* 1990). If micas are sufficiently close together, mechanical interactions between neighboring mica pairs may further perturb stresses locally, with the degree of stress concentration depending critically upon the spacing of grains relative to their length. In a similar way, interactions may be expected between neighboring multigranular clusters. These clusters may act as large mode II shear flaws, and interaction between an individual pair of clusters depends upon the local values of L_c and L_b.

Ductile-shear mechanical response in the $x45z$ orientation occurs in samples in which shear zones localize within prominent mica segregations across much of the sample. Samples in this deformation regime include those that contain a pervasive network of thin, wavy mica films (Fig. 3d), and those with more nearly-planar mica seams (Figs. 3e & f). Maximum LMC measurements for some ductile shear samples are similar to those for samples showing transitional response (Fig. 15); thus, this parameter does not adequately distinguish between textures characterized by interconnected mica films and those comprised of closely spaced isolated mica clusters. However, LMC measurements do appear to discriminate between segregations comprised of anastomosing mica films and those with nearly-planar geometries, since samples with planar seams consistently have lower strengths and yield higher LMC_{max} values. The low strengths of samples with planar seams suggest that ductile shear zones are better able to follow less tortuous paths across a sample, and measurements of LMC provide one means for predicting strength differences among samples containing interconnected mica domains of varying tortuosity.

The strengths of samples that developed ductile shear zones may also be influenced by the preferred orientations of micas within the zones in which strain localization actually occurred, with sample strengths decreasing with increasing preferred orientation. Measurements of mica preferred orientations for the Riggins Formation schist (Fig. 5) indicate that micas are more closely aligned parallel to S within mica-rich seams than in bulk. In all $x45z$ samples of Riggins Formation schist tested shear zones nucleated in these seams, and their low strength may be associated with the strong preferred orientations of mica in these seams as well as their high mica contents. A variety of other microstructural parameters that we have not considered here may be important to the mechanical response of mica-bearing rocks, and a complete understanding of the response of foliated rocks loaded at angles to S may ultimately require finite element analyses that consider the rheologies and complex configurations of the constituent phases (Tullis *et al.* 1991).

Models of anisotropy

Without developing numerical models that incorporate the statistical arrangement of micas, it is not possible to predict rigorously the strengths or anisotropies of mica-rich rocks. Nonetheless, microstructural parameters identified in this study provide a mechanistic understanding for existing phenomenological models of mechanically-anisotropic rocks (e.g. Jaeger 1960, Walsh & Brace 1964, McLamore & Gray 1967, Pariseau 1972, Ashour 1988, Karr *et al.* 1989), and suggest the fabric elements that lead to anisotropic or isotropic response. The range of anisotropy coefficients defined by the experiments reported here (Fig. 8) are similar to the range suggested by the combined results of previous studies, with different starting materials exhibiting both strongly anisotropic and nearly-isotropic response. In addition, sample-scale modes of deformation are similar to those reported previously, with strains localized in shear zones that cross-cut S at high angles in z orientation samples (shortened normal to S) and shear zones that form parallel or at low angles to S in samples shortened at 45° to foliation (orientation $x45z$). However, the mechanisms responsible for strain localization in shear zones are varied. The degree and type of mechanical anisotropy exhibited by a given starting material loaded in different orientations depends on rock fabric, which influences the degree to which strength and modes of deformation vary with β. Strengths and relative anisotropies of samples that were shortened at both 45° and 90° to foliation are shown in Fig. 16, and their corresponding stress–strain behaviors (i.e. brittle, transitional and ductile shear) and mica preferred orientations are compared. The great diversity of mechanical response revealed by these results suggests that no single description of mechanical anisotropy (as shown in Fig. 2) can explain the full range of behavior observed.

Several samples loaded in the $x45z$ orientation developed ductile shear zones parallel to S, as required by models that treat foliation as a unique plane of weakness. At relatively low mica contents, planes of interconnected micas will only be present in rocks with extreme segregation of micas into discrete, widely spaced seams (e.g. Honey Formation II and Sandy Formation). In

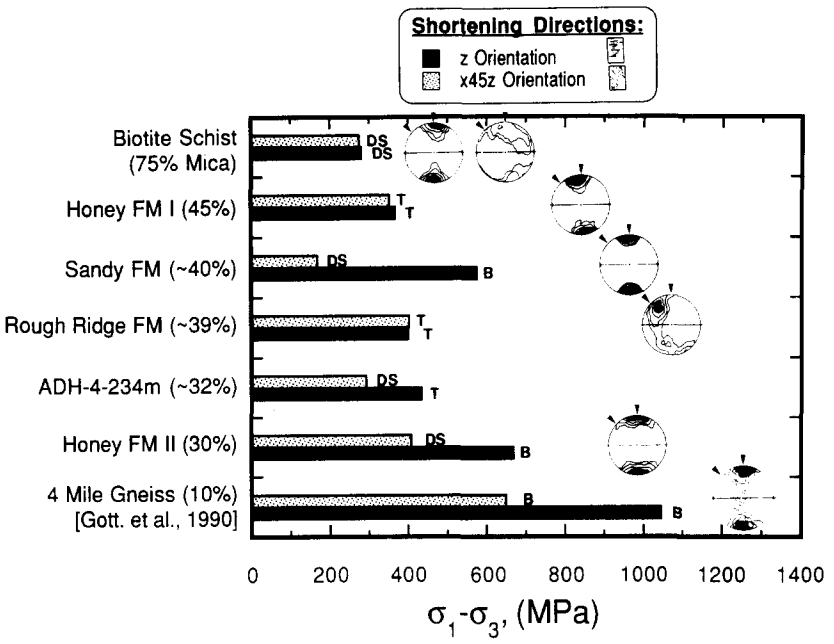

Fig. 16. Comparison of strength and degree of anisotropy for foliated rocks shortened at 45° and 90° to S (orientations $x45z$ and z, respectively). The stress–strain responses characteristic of these samples are labeled brittle (B), transitional (T) and ductile shear (DS). Simplified contour plots of poles to mica {001} (after Fig. 5) are included for those starting materials for which preferred orientations were measured (compression directions shown by arrows). Results for Four Mile gneiss (Gottschalk *et al.* 1990) are shown for comparison. Mechanical anisotropy does not correlate uniquely with strength of preferred orientation, particularly in those rocks with high mica content (i.e. ≥40 vol %).

these materials, the stresses required for slip along segregation (and parallel to S) are expected to be lower than those needed for fracture across strong, brittle interlayers for a wide range of intermediate β values. At extreme values of β (i.e. near 0° and 90°) shear zones cannot make use of interconnected mica seams. Samples in these orientations are stronger (as observed for z orientation samples) and exhibit brittle stress–strain response. As a result of marked contrasts in mode of strain localization as a function of orientation (Fig. 16), anisotropy coefficients are large.

Samples of low to intermediate mica content that exhibited brittle and transitional response (Table 1) developed shear zones at angles to S, which transected both mica clusters (parallel to S) and resistant bridges of stronger phases (at 5–20° to σ_1)(Figs. 12a & b). Similar shear zone geometries have been described in other rock types with low to intermediate mica contents (Borg & Handin 1966, Gottschalk *et al.* 1990). These characteristic, stepped shear zone geometries suggest that failure in samples with isolated mica clusters occurred through interactions between inclined micas and microcracks in the resistant silicates, rather than along a discrete plane with anomalous physical properties. These rocks do not possess interconnected networks of micas along planes of any orientation through the rock mass, and their mechanical response (at the experimental conditions tested) is likely to be either brittle or transitional for any value of β. Shear zones inclined to S may propagate by similar mechanisms for all loading directions, as observed by Gottschalk *et al.* (1990) for gneiss, and the shear zone angle may vary continuously as a function of orientation, as predicted by theories that assume continuously varying anisotropy (Jaeger 1960, McLamore & Gray 1967, Donath 1972, Pariseau 1972, Ashour 1988, Karr *et al.* 1989). The mechanical anisotropies of these rocks may be explained by simple models involving tensile crack nucleation within the brittle silicates ahead of and between mica grains oriented for kinking or slip and frictional sliding along {001}, as proposed by Gottschalk *et al.* (1990). Alternatively, the response of rocks with low to intermediate mica content or with preferred orientations inclined to the composition foliation may be more nearly isotropic, as shown by the results for Rough Ridge Formation samples (Fig. 16).

Discrete mica seams and interlayers were present in many samples of higher mica content, but interseam domains in these rocks typically have moderate mica concentrations. Although the segregation seams in these rocks constitute weak links across samples, the variation in mica contiguity as a function of β may not be as pronounced as in rocks with more distinct differentiated layering. As a result, failure within mica seams parallel to S may only occur for a limited range of high shear stress orientations (i.e. values of β close to 45°). At other values of β, shear zones may propagate through the coalescence of micro-kink bands in interconnected micas along planes at shallow angles to S (Fig. 10d), or by mechanisms involving simultaneous plastic deformation of micas and microcracking in surrounding phases (Fig. 10c). These rocks may also display continuously varying anisotropy, but the functional form of their strength vs β curves may differ significantly from that defined by results for rocks of lower mica content. Although the exact form of these curves cannot be predicted on the basis of results for samples shortened at 45° and 90° to foliation alone, the low anisotropy coefficients determined for samples containing high concen-

trations of evenly-dispersed micas (e.g. NSF Drill Hole 4—234 m; Figs. 8 and 16) suggest that their strengths may not vary as much with orientation as the strengths of starting materials with strongly differentiated textures.

The most mica-rich schist examined in this study, the Riggins Formation biotite schist (75% mica by volume), developed steady-strength ductile shear zones when loaded in both the z and $x45z$ formations. In these orientations, shear zones localized through the nucleation and coalescence of dense sets of micro-kink bands. Despite distinct differences in the relative number of micas oriented favorably for slip and kinking in different orientations (Fig. 5), the schist's mechanical response was nearly isotropic. Mica contiguity is high along all planes through the rock, and its lack of anisotropy suggests that the strength of highly micaceous rocks may be relatively insensitive to averaged {001} orientations, provided the concentration of grains oriented favorably for slip and kinking exceeds some critical density. The relatively low strength of the Hartland Formation schist (~60% mica) loaded normal to S supports this conclusion (Fig. 6c). Like the Riggins Formation schist, it contains a significant population of micas oriented for easy slip and kinking in nearly all loading directions (Fig. 5). Isotropic response also occurs in the Honey Formation I schist, which possesses a somewhat lower concentration of micas (~45 vol %) with a much stronger preferred orientation than either the Riggins or Hartland Formation schists. This result suggests that isotropic response may be favored in rocks with high mica contents, irrespective of the strength of mica preferred orientation.

Effects of scale

The mechanical properties of the rocks tested in this study appear to depend critically upon the dimensions of interconnected mica segregations relative to the dimensions of the experimental samples used, particularly when they are loaded at 45° to S. For this sample orientation, the lengths of individual mica clusters in many starting materials typically approach or exceed the 8 mm diameter of the cores tested, and the strengths and stress–strain behaviors of these samples (which deform by ductile shear) contrast sharply with the response exhibited by samples with much shorter cluster lengths (Fig. 14a). Mica contiguity and thus the modes of deformation depend upon sample size for a given starting material. Linear mica continuity (LMC), characteristic mica cluster dimensions and quartzo-feldspathic bridge dimensions have all been defined and reported relative to the sample size. Thus, the general correlations that we have established between mechanical response and key microstructural parameters (Figs. 14 and 15) should be applicable over a range of sample sizes, provided the parameters are normalized to the scale being considered.

At the outcrop scale (and even larger scales) the mechanical response may be influenced by the geometry of layer silicate segregations and the continuity of micas along planes oriented for shear. Foliated, mica-rich shear zones with lengths ranging from several meters to tens of kilometers have been described in granitic host rocks from a number of tectonic settings (Janecke & Evans 1988, O'Hara 1988, Gibson 1990, Zulauf *et al.* 1990). These shear zones may range in thickness from centimeters to hundreds of meters, and meso-scale and microstructural observations from their interiors indicate that foliations are defined by spaced mica segregations up to several centimeters wide alternating with host rock domains of similar dimensions. Kinematic indicators (e.g. oblique grain-shape fabrics, shear bands, and pressure shadows of non-phyllosilicate phases) indicate that the deformation history in many shear zones is approximately one of simple shear, and the geometry and orientation of phyllosilicate seams suggest that they are commonly aligned in orientations that resulted in high shear stresses resolved along them. As a result, the mechanical response of these zones will almost certainly be influenced by the contiguity of micas parallel to the shear zone boundaries. In many phyllonites (e.g. those described by Janecke & Evans 1988 and Gibson 1990) mica concentrations appear to be relatively high; when loaded tectonically at shallow crustal conditions, these zones may behave as long, relatively weak inclusions in a stronger (i.e. granitic) host.

Gibson (1990) has documented both dilatant sites and zones of localized compression at the stepovers between adjacent mica seams in phyllonites that cross-cut Proterozoic quartzo-feldspathic gneisses, and suggested that these zones are analogous to those generated between en échelon faults (Segall & Pollard 1980, Gamond 1983). Sibson (1989) has suggested that fracture within stepovers in zones of active faulting may allow several short segments to link together and accommodate larger displacements, while cementation of these bridges may occur following an episode of seismic fault slip. Similar bridges may be present at the terminations of outcrop and larger-scale spaced en échelon micaceous faults and shear zones at depth, with stepover zones consisting primarily of quartz and feldspars. The local stresses required to rupture quartzo-feldspathic bridges and transfer slip between adjacent micaceous shear zones are likely to depend upon the nearest-neighbor spacing of these zones relative to their length, much as observed at a smaller scale in rocks of low-to-intermediate mica content that were tested in this study.

CONCLUSIONS

At conditions of temperature, pressure and strain rate at which micas are weak relative to other strong silicates, the mechanical properties of foliated rocks depend in a complex way upon the concentrations, preferred orientations and spatial arrangements of micas. Strengths and mechanical anisotropies exhibited by a collection of schist and gneiss samples shortened at 45° and 90° to foliation (S) at $T = 25°C$, $P_c = 200$ MPa and a strain rate of $\sim 10^{-5}$ s^{-1} were correlated with both initial micro-

structural variables and deformation microstructures that developed during the experiments. The results of these experiments and observations lead to the following conclusions.

(1) Strains in all samples localized within discrete sub-mm to mm wide shear zones, and were accommodated by dislocation slip and grain-scale microkinking in micas, and cataclasis of stronger phases. Shear zone formation in both $x45z$ and z oriented samples was associated either with discrete stress drops immediately after the peak stress (brittle fracture), stable-strain softening (transitional response) or steady-strength flow in ductile shear zones. Peak compressive strengths of samples shortened at 45° and 90° to S varied by factors of 6 and 4, respectively.

(2) Three modes of strain localization have been identified from microstructural observations. These coincide with the regimes of brittle, transitional and ductile shear defined on the basis of stress–strain response. In brittle and transitional samples, shear zone geometries show close geometrical relationships with plastically deformed micas, but extensive microcracking of strong silicate bridges is required to generate shear fractures and shear zones. Transitional response is favored over brittle fracture with increasing length or decreasing spacing of isolated mica clusters along planes oriented for shear, and is associated with mechanical processes of phase redistribution which increase the contiguity of micas in the shear plane. Ductile shear zones are accommodated largely by distributed slip and kinking within inclined zones of interconnected micas.

(3) Samples shortened in both the $x45z$ and z orientations show trends of decreasing strength and increasing ductility with increasing bulk mica content, but both strength and ductility correlate more directly with the initial contiguity of micas along planes of high shear stress, along which fractures and shear zones may form. In z orientation samples, failure occurs along planes at high angles to S for which contiguity is similar to bulk mica content; the mechanical behavior of these samples can be predicted effectively from mica concentration alone.

(4) For $x45z$ orientation samples, strength and ductility can be correlated most directly with relatively simple microstructural measurements of: (i) the maximum concentration of micas along shear zone-parallel traverses across samples; (ii) the maximum length of multigranular mica clusters (normalized to sample dimensions); and (iii) the dimensions of quartzo-feldspathic bridges between mica clusters (normalized to sample dimensions and cluster size). Foliations in most samples are defined by aligned mica clusters or longer, discrete mica segregations. When these segregations are aligned at 45° to the shortening direction (orientation $x45z$) they represent weak links across samples, and the mechanical behavior of $x45z$ samples reflects the properties along the most mica-rich planes parallel to foliation, rather than the bulk textures and compositions of starting materials.

(5) Anisotropy coefficients defined as ratios of compressive strengths of z orientation and $x45z$ orientation samples $[\sigma_d(z)/\sigma_d(x45z)]$ range from 1 (isotropic response) to 4. Correlations of these coefficients with microstructures in deformed samples suggest that no single model of anisotropic behavior is consistent with the strain localization mechanisms observed. In samples with low mica contents (i.e. <20%) and strong preferred orientations, mechanical anisotropies stem from differences in the relative concentrations of shear flaws (i.e. mica clusters inclined to σ_1) in different sample orientations. This anisotropy may be described best by models that assume a continuous variation of strength with β (the angle between σ_1 and S). With increasing mica content, anisotropy coefficients correlate more directly with the orientations of mica-rich seams and mica contiguity. Isotropic response is favored in samples in which contiguity does not vary strongly with orientation, while strongly anisotropic response is exhibited by samples with heterogeneous dispersions of micas and other, stronger phases. Unique plane-of-weakness models of anisotropy are most appropriate for mica-rich rocks with throughgoing, alternating mica-rich and mica-poor lamina. In rocks in which prominent mica seams occur within a micaceous matrix, shear zones may form at angles to S, at differential stresses that are similar to those required for slip along the seams. Depending upon mica contents within the matrix, these rocks may show weak, continuously varying anisotropies or nearly-isotropic response.

Acknowledgements—This study was supported by the U.S. Department of Energy, grant No. DE-FG05-87ER13711. W. Shea is also grateful for financial support provided by the Center for Tectonophysics and Department of Geology at Texas A&M University. We thank Nikolas Christensen and his research team at Purdue University, who allowed us access to the NSF Appalachian Drill Cores and assisted with sample selection. We also thank Will Lamb, who helped with the selection of samples from the Llano region of central Texas, and Rick Gottschalk, who provided us with thin sections of his deformed gneiss samples. Buckey Turk and Jack McGouirk assisted us with the rock deformation experiments, and we thank Robin McNeely for preparation of still another manuscript. We benefitted from discussions with J. Handin, N. Carter, M. Friedman and D. Wiltschko, and thank G. Hirth, J. Tullis and an anonymous reviewer for their insightful reviews.

REFERENCES

Ashour, H. A. 1988. A compressive strength criterion for anisotropic rock materials. *Can. Geotech. J.* **25**, 233–237.

Bell, I. A. & Wilson, C. J. L. 1981. Deformation of biotite and muscovite: TEM microstructure and deformation model. *Tectonophysics* **78**, 201–228.

Bell, I. A., Wilson, C. J. L., McLaren, A. C. & Etheridge, M. A. 1986. Kinks in mica: Role of dislocations and (001) cleavage. *Tectonophysics* **127**, 49–65.

Bons, A. J. 1988. Deformation of chlorite in naturally deformed low-grade rocks. *Tectonophysics* **154**, 149–165.

Borg, I. & Handin, J. W. 1966. Experimental deformation in crystalline rock. *Tectonophysics* **3**, 251–323.

Burg, J.-P. & Wilson, C. J. L. 1987. Deformation of two phase systems with contrasting rheologies. *Tectonophysics* **135**, 199–205.

Christensen, N. I. & Szymanski, D. L. 1988. Origin of reflections from the Brevard fault zone. *J. geophys. Res.* **93**, 1087–1102.

Christoffersen, R. & Kronenberg, A. K. 1993. Dislocation interactions in experimentally deformed biotite. *J. Struct. Geol.* **15**, 1077–1095.

Deklotz, E. J., Brown, J. W. & Stemler, O. A. 1966. Anisotropy of a schistose gneiss. *Proc. First Cong. Int. Soc. Rock Mech.*, 369–379.

Donath, F. A. 1961. Experimental study of shear failure in anisotropic rocks. *Bull. geol. Soc. Am.* **72**, 985–990.

Donath, F. A. 1964. Strength variation and deformational behavior in anisotropic rock. In: *State of Stress in the Earth's Crust* (edited by Judd, W. R.). American Elsevier, New York, 281–298.

Donath, F. A. 1972. Effects of cohesion and granularity on deformational behavior of anisotropic rock. In: *Studies in Mineralogy and Precambrian Geology* (edited by Doe, B. R. & Smith, D. K.). *Mem. geol. Soc. Am.* **135**, 95–128.

Etheridge, M. A., Hobbs, B. E. & Paterson, M. S. 1973. Experimental deformation of single crystals of biotite. *Contr. Miner. Petrol.* **38**, 21–36.

Evans, J. P. 1988. Deformation mechanisms in granitic rocks at shallow crustal levels. *J. Struct. Geol.* **10**, 437–443.

Evans, J. P. 1990. Textures, deformation mechanisms, and the role of fluids in the cataclastic deformation of granitic rocks. In: *Deformation Mechanisms, Rheology, and Tectonics* (edited by Knipe, R. J. & Rutter, E. H.). *Spec. Publs geol. Soc. Lond.* **54**, 29–39.

Gamond, J. F. 1983. Displacement features associated with fault zones: a comparison between observed examples and experimental models. *J. Struct. Geol.* **5**, 33–45.

Gibson, R. G. 1990. Nucleation and growth of retrograde shear zones: an example from the Needle Mountains, Colorado, U.S.A. *J. Struct. Geol.* **12**, 339–350.

Goodwin, L. B. & Wenk, H.-R. 1990. Intracrystalline folding and cataclasis in biotite of the Santa Rosa mylonite zone: HVEM and TEM observations. *Tectonophysics* **172**, 201–214.

Gottschalk, R. R., Kronenberg, A. K., Russell, J. E. & Handin, J. 1990. Mechanical anisotropy of gneiss: Failure criterion and textural sources of directional behavior. *J. geophys. Res.* **95**, 21,613–21,634.

Handy, M. R. 1990. The solid-state flow of polymineralic rocks. *J. geophys. Res.* **95**, 8647–8661.

Hobbs, B. E., Means, W. D. & Williams, P. F. 1976. *An Outline of Structural Geology*. John Wiley, New York.

Jaeger, J. C. 1960. Shear failure of anisotropic rocks. *Geol. Mag.* **97**, 65–72.

Janecke, S. U. & Evans, J. P. 1988. Feldspar-influenced rock rheologies. *Geology* **16**, 1064–1067.

Jordan, P. 1987. The deformational behavior of bimineralic limestone-halite aggregates. *Tectonophysics* **133**, 185–197.

Jordan, P. 1988. The rheology of polymineralic rocks: An approach. *Geol. Rdsch.* **77**, 285–294.

Kamb, W. B. 1959. Ice petrofabric observations from Blue glacier, Washington, in relation to theory and experiment. *J. geophys. Res.* **64**, 1891–1909.

Kanaori, Y., Kawakami, S. & Yairi, K. 1991. Microstructure of deformed biotite defining foliation in cataclasite zones in granite, central Japan. *J. Struct. Geol.* **13**, 777–785.

Karr, G. G., Law, F. P. & Hoo Fatt, M. 1989. Asymptotic and quadratic failure criteria for anisotropic materials. *J. Plastic.* **5**, 303–336.

Kronenberg, A. K., Kirby, S. H. & Pinkston, J. C. 1990. Basal slip and mechanical anisotropy of biotite. *J. geophys. Res.* **95**, 19257–19278.

Logan, J. M. & Rauenzahn, K. A. 1987. Frictional dependence of gouge mixtures of quartz and montmorillonite on velocity, composition, and fabric. *Tectonophysics* **144**, 87–108.

Mares, V. M. & Kronenberg, A. K. 1993. Experimental deformation of muscovite, *J. Struct. Geol.* **15**, 1061–1075.

McCabe, W. M. & Koerner, R. M. 1975. High pressure shear strength investigation of an anisotropic mica schist rock. *Int. J. Rock Mech. Min. Sci. & Geomech. Abs.* **12**, 219–228.

McLamore, R. & Gray, K. E. 1967. The mechanical behavior of anisotropic sedimentary rocks. *J. Engng Ind.* **89**, 62–76.

O'Hara, K. 1988. Fluid flow and volume loss during mylonitization: an origin for phyllonite in an overthrust setting. North Carolina, U.S.A. *Tectonophysics* **156**, 21–36.

Pariseau, W. G. 1972. Plasticity theory for anisotropic rocks and soils. *Proc. 10th Symp. Rock Mech.* 267–295.

Paterson, M. S. & Weiss, L. E. 1966. Experimental deformation and folding in phyllite. *Bull. geol. Soc. Am.* **77**, 343–374.

Peng, S. & Johnson, A. M. 1972. Crack growth and faulting in cylindrical specimens of Chelmsford granite. *Int. J. Rock Mech. Min. Sci. & Geomech. Abs.* **9**, 37–86.

Price, R. H. 1982. Effects of anhydrite and pressure on the mechanical behavior of synthetic rocksalt. *Geophys. Res. Lett.* **9**, 1029–1032.

Ross, J. V., Bauer, S. J. & Hansen, F. D. 1987. Textural evolution of synthetic anhydrite-halite mylonites. *Tectonophysics* **140**, 307–326.

Segall, P. & Pollard, D. D. 1980. Mechanics of discontinuous faults. *J. geophys. Res.* **85**, 4337–4350.

Shea, W. T. & Kronenberg, A. K. 1992. Rheology and deformation mechanisms of an isotropic mica schist. *J. geophys. Res.* **97**, 15,201–15,237.

Sibson, R. H. 1989. Earthquake faulting as a structural process. *J. Struct. Geol.* **11**, 1–14.

Tapponnier, P. & Brace, W. F. 1976. Development of stress-induced microcracks in Westerly granite. *Int. J. Rock Mech. Min. Sci. & Geomech. Abs.* **13**, 103–112.

Tharp, T. M. 1983. Analogies between the high-temperature deformation of polyphase rocks and the mechanical behavior of porous powder metal. *Tectonophysics* **96**, T1–T11.

Tullis, J. & Yund, R. A. 1977. Experimental deformation of Westerly granite. *J. geophys. Res.* **82**, 5705–5718.

Tullis, T. E., Horowitz, F. G. & Tullis, J. 1991. Flow laws of polyphase aggregates from end-member flow laws. *J. geophys. Res.* **96**, 8081–8096.

Vernon, R. H., Williams, V. A. & D'Arcy, W. F. 1983. Grain-size reduction and foliation development in a deformed granitoid batholith. *Tectonophysics* **92**, 123–145.

Walsh, J. B. & Brace, W. F. 1964. A fracture criterion for brittle anisotropic rock. *J. geophys. Res.* **69**, 3449–3456.

Wawersik, W. R. & Brace, W. F. 1971. Post-failure behavior of a granite and diabase. *Rock. Mech.* **3**, 61–85.

Williams, R. T., Hatcher, R. D., Coruh, C., Costain, J. K., Zoback, M. D., Anderson, R. N., Diebold, J. B. & Phinney, R. A. 1987. The southern Appalachian ultradeep scientific drill hole: Progress of site location investigations and other recent developments. In: *Observation of the Continental Crust Through Drilling, Vol.* 2 (edited by Behr, H. J., Staley, F. G. & Vidal, H.). Springer, New York, 44–55.

Wilson, C. J. L. & Bell, I. A. 1979. Deformation of biotite and muscovite: Optical microstructure. *Tectonophysics* **58**, 179–200.

Wong, T.-f. 1982. Micromechanics of faulting in Westerly granite. *Int. J. Rock Mech. Min. Sci. & Geomech. Abs.* **19**, 49–64.

Wong, T.-f. & Biegel, R. 1985. Effects of pressure on the micromechanics of faulting in San Marcos gabbro. *J. Struct. Geol.* **7**, 737–749.

Zulauf, G. F., Kleinschmidt, G. & Oncken, O. 1990. Brittle deformation and graphitic cataclasites in the pilot research well KTB-VB (oberpfalz, FRG). In: *Deformation Mechanisms, Rheology, and Tectonics* (edited by Knipe, R. J. & Rutter, E. H.). *Spec. Publs. geol. Soc. Lond.* **54**, 97–103.